

A review of progress in thermo-mechanical energy storage technologies for combined cooling, heating and power applications

Jiaxing Huang¹, Yao Zhao (✉)^{1,2}, Jian Song^{3,4}, Shengqi Huang¹, Kai Wang^{5,6}, Zhenghua Rao⁷, Yongliang Zhao⁸, Liang Wang⁹, Xi Wan¹, Yue Fei¹, Christos N. Markides⁴

¹ College of Smart Energy, Shanghai Jiao Tong University, Shanghai 200240, China

² Shanghai Non-carbon Energy Conversion and Utilization Institute, Shanghai Jiao Tong University, Shanghai 200240, China

³ Birmingham Centre for Energy Storage & School of Chemical Engineering, University of Birmingham, Birmingham B15 2TT, UK

⁴ Clean Energy Processes (CEP) Laboratory, Department of Chemical Engineering, Imperial College London, London SW7 2AZ, UK

⁵ Institute of Refrigeration and Cryogenics, Zhejiang University, Hangzhou 310027, China

⁶ Key Laboratory of Refrigeration and Cryogenic Technology of Zhejiang Province, Zhejiang University, Hangzhou 310027, China

⁷ School of Energy Science and Engineering, Central South University, Changsha 410083, China

⁸ State Key Laboratory of Multiphase Flow in Power Engineering, Xi'an Jiaotong University, Xi'an 710049, China

⁹ Institute of Engineering Thermophysics, Chinese Academy of Sciences, Beijing 100190, China

© Higher Education Press 2025

Abstract Thermo-mechanical energy storage (TMES) technologies have attracted significant attention due to their potential for grid-scale, long-duration electricity storage, offering advantages such as minimal geographical constraints, low environmental impact, and long operational lifespans. A key benefit of TMES systems is their ability to perform energy conversion steps that enable interaction with both thermal energy consumers and prosumers, effectively functioning as combined cooling, heating and power (CCHP) systems. This paper reviews recent progress in various TMES technologies, focusing on compressed-air energy storage (CAES), liquid-air energy storage (LAES), pumped-thermal electricity storage (PTES, also known as Carnot battery), and carbon dioxide energy storage (CES), while exploring their potential applications as extended CCHP systems for trigeneration. Techno-economic analysis indicate that TMES-based CCHP systems can achieve roundtrip (power-to-power) efficiencies ranging from 40% to 130%, overall (trigeneration) energy efficiencies from 70% to 190%, and a levelized cost of energy (with cooling and heating outputs converted into equivalent electricity) between 70 and 200 \$/MWh. In general, the evolution of TMES-based CCHP systems into smart multi-energy management systems for cities or districts in the future is a highly promising avenue. However, current economic analyses remain incomplete, and further exploration is needed, especially in the area “AI for energy storage,” which is crucial for the widespread adoption of TMES-based CCHP systems.

Keywords thermo-mechanical energy storage (TMES), combined cooling, heating and power, compressed-air energy storage (CAES), liquid-air energy storage (LAES), pumped-thermal energy storage (PTES), carbon dioxide energy storage (CES)

1 Introduction

1.1 Background and concept

Energy storage technologies have witnessed rapid development in recent decades, driven by the growing

integration of renewable energy generation [1,2]. The most mature large-scale energy storage technology is pumped-hydro storage (PHS), which offers high roundtrip efficiencies (> 75%) and storage durations ranging from hours to days. However, PHS is limited by geographical and geological factors, restricting its further deployment potential in many regions. Electrochemical batteries such as lithium-ion, lead-acid, are also widely used for energy storage due to their advantages of rapid response, high efficiency, and excellent ability for

Received Nov. 4, 2024; accepted Feb. 12, 2025; online Mar. 30, 2025

Correspondence: Yao Zhao, zhaoyao@sjtu.edu.cn

Special Issue: Thermo-mechanical Energy Storage Technologies

modular deployment. Despite significant recent progress, the lifespan of these batteries remains relatively limited, with high lifetime and lifecycle costs. Additionally, environmental impact and security concerns continue to present challenges [3,4].

In this context, and specifically for larger-scale and longer-duration storage, thermo-mechanical energy storage (TMES) technologies have garnered attention thanks to their favorable environmental impact, cost-effectiveness, and extended lifespans, among other advantages. TMES systems store energy by converting electrical or mechanical energy into thermal energy, and release it by converting the stored thermal energy back into electrical or mechanical energy. This process inherently involves the flow of various forms of energy into and out of the systems. TMES systems typically consist of mechanical components (such as compressors and expanders), heat exchangers, and storage units. Based on their operating principles, the most common TMES technologies can be broadly categorized into four types: compressed-air energy storage (CAES) [5–7], liquid-air energy storage (LAES) [8,9], pumped-thermal energy storage (PTES) [10,11], and carbon dioxide energy storage (CES) [12,13], all of which are the subject of extensive research at present.

- **CAES** is the most mature option among TMES options. In CAES systems, electrical energy is used to drive compressors for compressing air, which is then stored at high pressure, thus completing the conversion from electrical to mechanical energy. In certain configurations, such as adiabatic CAES, the heat released during compression is recovered, stored, and later used during discharge to preheat the high-pressure air before it expands in turbines [14,15].

- **LAES** has now reached an advanced stage of development and demonstration. Typical LAES systems comprise three storage components: one for near-ambient pressure liquefied air, one for compression heat, and one for high-grade cold energy. During charging, the air is compressed, cooled, and throttled to produce liquefied air at near-ambient pressure for storage. During discharging, the stored liquefied air is pressurized, vaporized, heated, and expanded through turbines to generate electricity [16–18].

- **PTES**, also called Carnot battery, is still in the early stages of development and demonstration. PTES systems utilize a heat pump cycle to convert electrical energy into thermal energy for storage during charging. During discharging, the stored thermal energy is converted back into electricity through a power cycle [19–23].

- **CES** which is also in the early stage of demonstration, operates on a principle similar to that of CAES, but with CO₂ instead of air. CO₂ is susceptible to liquefaction and can be stored in either a liquid or a supercritical state. During charging, CO₂ is compressed by compressors and stored in high-pressure tanks. During discharging, the

stored CO₂ is vaporized, heated, and expanded through turbines to generate electricity [24].

The concepts, principles, and potential of TMES technologies have been extensively reviewed in literature. For example, Steinmann [25] provided an overview of the basic concepts and characteristics of TMES systems, exploring their potential for waste heat utilization and integration with power plants. Olympios et al. [26] conducted a techno-economic analysis of TMES technologies, and explored their competitiveness, comparing them with PHS, vanadium redox flow batteries, and lithium-ion batteries. They found that TMES systems could achieve roundtrip efficiencies exceeding 60%, with lifespans over 30 years and energy capital costs below 100 \$/kWh for higher discharge power ratings and longer discharge durations. Many other studies have attempted to provide a comparative overview of multiple TMES options, focusing on specific technologies, such as those for CAES [27–30], LAES [31–35], and PTES [36–39].

Recently, combined cooling, heating, and power (CCHP) systems have garnered increased attention from both academia and industry thanks to their notable advantages, including high efficiency, economic benefits, and lower greenhouse gas emissions [40]. However, these traditional CCHP systems, centered around power generation units (PGUs), still rely on fuel combustion for power generation [41]. In contrast, TMES systems can generate thermal energy during charging and/or discharging by utilizing renewable energy sources, allowing them to deliver both electrical and thermal energy to cater to external energy demands in these systems [42]. Such TMES-based CCHP systems (Fig. 1) offer flexibility of meeting multiple energy demands, and can integrate with waste heat (or cold) through external streams, either directly with the system processes or through thermal energy storage (TES) units, thereby increasing overall efficiency and economic benefits. Besides, the inclusion of TES units in TMES-based CCHP systems enables energy transfer not only across energy vectors but also over time, making them adaptable and capable of evolving into smart energy management solutions for future urban and district applications. Despite the growing interest in TMES systems, existing reviews have primarily focused on specific TMES technologies or their standalone applications, lacking a comprehensive exploration of their potential as CCHP systems.

This paper offers a comprehensive and systematic review of recent advancements in TMES technologies, specifically focusing on their applications in CCHP systems. It also discusses the thermodynamic principles underlying these TMES-based CCHP systems and outlines the latest developments in their design and implementation. A unique contribution of this work is its in-depth comparison of various TMES-based CCHP systems, highlighting both the thermodynamic and

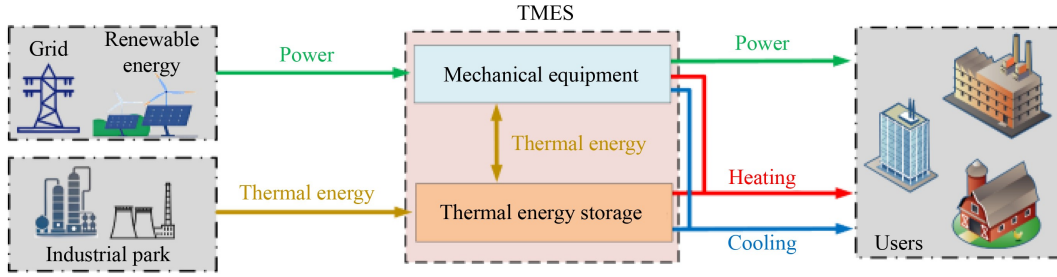


Fig. 1 Diagram of energy flows in TMES-based CCHP systems.

economic metrics to assess their potential as reliable and cost-effective solutions.

The applications of CAES, LAES, PTES and CES technologies for CCHP are, respectively, summarized in Sections 2, 3, 4 and 5. Section 6 synthesizes these findings, providing a comparative analysis and discussing the application of these systems across different sectors. The final section explores future development prospects, offering insights into how TMES-based CCHP systems can evolve into advanced energy management technologies that contribute to sustainable development. This review aims to bridge existing gaps and propose directions for research and implementation that could drive the continued evolution of TMES-based CCHP systems in the years to come.

1.2 Performance indicators

Various indicators can be used to evaluate TMES-based CCHP technologies based on both thermodynamic and economic performance. One of the most commonly used metrics for assessing the thermodynamic performance of TMES energy storage systems is the roundtrip (power-to-power) efficiency (RTE), denoted as η_{rt} . RTE is defined as the ratio of total power output to total power input in TMES-based CCHP systems [25,26]

$$\eta_{rt} = \frac{E_{\text{output}}}{E_{\text{input}}}, \quad (1)$$

where E_{input} and E_{output} are the input electrical energy during charging, and output electric energy during discharging, respectively.

In CCHP systems, where a net amount of thermal energy (hot and/or cold) can also be delivered during discharging, an overall trigeneration energy efficiency (TEE) η_{tri} can be defined as [33,43]

$$\eta_{tri} = \frac{E_{\text{output}} + Q_{\text{heat}} + Q_{\text{cold}}}{E_{\text{input}}}, \quad (2)$$

where Q_{heat} and Q_{cold} are the (net) hot and cold thermal energy vectors delivered by the system. This metric is also referred to in the literature as the overall efficiency, or the energy utilization factor (EUF).

Using this energy efficiency measure, based on the first law of thermodynamics, tends to overestimate the perfor-

mance of CCHP systems because it does not account for the varying levels or grades of thermal and electrical energy. To address this, the nominal-roundtrip efficiency (NRTE) is introduced, wherein the contributions of cooling and heating power are homogeneously converted into equivalent electricity, as defined below [33,44]

$$\eta_{nrt} = \frac{E_{\text{output}} + Q_{\text{heat}}/COP_{\text{heat}} + Q_{\text{cold}}/COP_{\text{cold}}}{E_{\text{input}}}, \quad (3)$$

where COP_{heat} and COP_{cold} are coefficients of performance for conversion from electricity to heating and cooling, which depend on the heating and cooling cycles employed.

Furthermore, based on the second law of thermodynamics, a total exergy efficiency η_{Ex} can be defined [33,45]

$$\eta_{Ex} = \frac{E_{\text{output}} + Ex_{\text{heat}} + Ex_{\text{cold}}}{E_{\text{input}}}, \quad (4)$$

where Ex_{heat} and Ex_{cold} are the heat and cold exergy outputs, respectively.

Turning to techno-economic measures of performance, the levelized cost of energy (LCOE) can be estimated as the cost of energy generated by the CCHP system over its lifetime, with cooling and heating outputs converted into equivalent electricity [33,46]

$$LCOE = \frac{TCC + \sum_{y=1}^n \frac{(C_{OM} + C_C)_y}{(1+r)^y}}{\sum_{y=1}^n \frac{(E_{\text{output}} + Q_{\text{heat}}/COP_{\text{heat}} + Q_{\text{cold}}/COP_{\text{cold}})_y}{(1+r)^y}}, \quad (5)$$

where TCC is the total capital cost of the system, C_{OM} is the combined operation and maintenance costs, C_C is the charging cost, y is the number of years over the system's lifetime, and r is the discount rate.

Additionally, the annual total profit (ATP) represents the difference between the income from trigeneration and the cost of purchasing electricity (input) purchase cost, which can be expressed as [33,46]

$$ATP = (C_{\text{peak}} E_{\text{output}} + C_{\text{heat}} Q_{\text{heat}} + C_{\text{cold}} Q_{\text{cold}}) - C_{\text{valley}} E_{\text{in}}, \quad (6)$$

where C_{peak} is the price of peak electricity, and C_{valley} is the price of valley electricity.

To assess the rate at which the initial investment in the

TMES can be recovered through cost savings or energy production, the static payback period (*SPP*) can be calculated as [33,46]

$$SPP = \frac{TCC}{ATP}, \quad (7)$$

and, considering the time value of capital, the dynamic payback period (*DPP*) from [33,46]

$$DPP = (y - 1) + \frac{|NPV_{y-1}|}{ATP_y}, \quad (8)$$

where *NPV* is the difference between cash inflows and outflows over a period, and (*y* - 1) is the last year when *NPV* < 0.

To account for inflation, economic data collected from different years are consistently converted using the Chemical Engineering Plant Cost Index (CEPCI) [47]

$$C_2 = C_1 \frac{I_2}{I_1}, \quad (9)$$

where *C*₁ and *C*₂ are the costs at base time and desired time, respectively; and *I*₁ and *I*₂ are the CEPCIs at base time and desired time, respectively. In this study, 2023 is chosen as the desired time, with a CEPCI value (*I*₂) of 797.9.

2 CAES for CCHP

2.1 Basic CAES-based CCHP system

This section focuses on the operation of a CAES system as a CCHP system, referred to as the basic CAES-based CCHP system, rather than integrating CAES technology into traditional coal-fired power plant-based CCHP systems, which rely on fuel-dependent steam turbines, gas turbines and other components [15,48].

Basic CAES-based CCHP systems are mainly composed of compressors, expanders (such as pneumatic motor [49]), air storage tanks, heat exchangers, inter-heaters, intercoolers, heat storage units, and valves, as shown in Fig. 2. The basic operating principle is summarized as follows: during charging, air is

compressed by multi-stage compressors and stored in air storage tanks. The resulting compression heat can either be recovered through intercoolers and stored in thermal energy storage or used directly for heating. During discharging, the compressed air is released from the air storage tanks, heated via inter-heaters, and then directed to the expander to do work. Cooling can be produced by adjusting the pressure and temperature of air at the expander inlet [50,51].

The heat storage temperatures in basic CAES-based CCHP systems are determined by the compression process. More compression stages typically result in lower compression heat temperatures, which usually range between 130 and 580 °C. The cooling temperature, on the other hand, is dictated by the expansion process, where a lower expander inlet temperature results in lower cooling temperatures, which can reach approximately -120 °C. Current studies primarily focus on applications such as space heating and hot water supply (with temperatures between 40 and 80 °C), as well as district cooling (with temperatures between -3 and 10 °C). However, the supply of high-grade heating and cooling from such basic CAES-based CCHP systems has yet to be reported.

The ratio of heating, cooling, and power supply in these systems can be adjusted according to demand. For instance, when charged with 97 kWh of electricity, a basic CAES-based CCHP system can produce 29 kWh of electricity, 100 kWh of heat energy, and 15 kWh of cold energy [52].

Preliminary assessments have been made regarding the potential of basic CAES-based CCHP systems for small buildings. Li et al. [53] conducted a case study on a small office building in Chicago and found that the NRTE could be around 50% in winter and 35% in summer, significantly higher than those of conventional CCHP systems based on absorption chilling technology. Similarly, Lv et al. [43] examined the economic, social, and technical performance of a basic CAES-based CCHP system in a typical five-star hotel in Shanghai. They found that the system operated efficiently under relatively low-pressure conditions (with air compressed and released at 15 bar), achieving an NRTE of 76% and

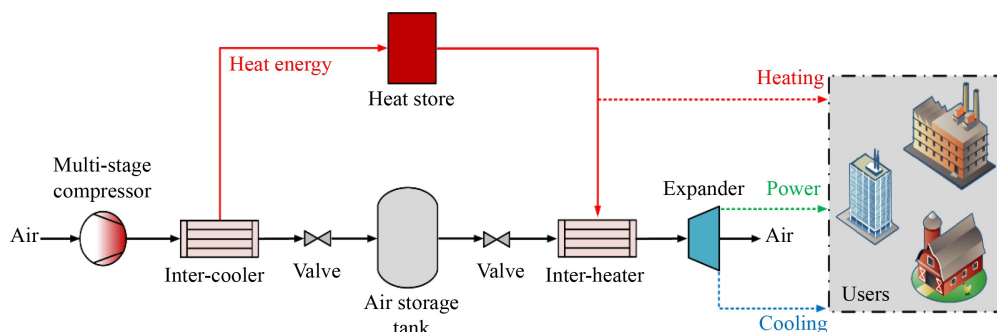


Fig. 2 Schematic diagram of basic CAES-based CCHP system.

reducing annual monetary costs by 54% compared to traditional CCHP systems using vapor compression refrigeration and heat pumps. For remote communities, Cheayb et al. [54] experimentally tested a simple configuration of a small 4 kW basic CAES-based CCHP system. The results showed that the RTE was extremely low at 3.6%, while the NRTE was slightly higher at 15.2%.

Research has also examined the impact of key design parameters on the performance of basic CAES-based CCHP systems. It was found that dividing the compression into two or three stages offers a good balance between RTE and system complexity, with at least three expansion stages required due to temperature limitations at the expander outlet. Increasing the air storage temperature negatively impacts RTE, with its capacity decreasing by 18% as the temperature rises from 30 to 100 °C [52]. Improving the inter-cooler and inter-heater effectiveness benefits RTE, but increasing inter-heater effectiveness negatively affects TEE [55]. This is because higher inter-heater effectiveness allows more stored heat to be utilized for turbine power generation, thereby reducing the heat available for heating. Additionally, the reduction in heating output is more significant than the increase in power generation, due to the inherently higher quality of electricity compared to heating energy.

In terms of the dynamic characteristics and operating modes of such basic CAES-based CCHP systems, Alsagri et al. [56] studied the impact of off-design operation on the performance of subcooled CAES-based CCHP system, and found that as the load decreased from 100% to 10%, RTE, power-to-cooling efficiency, power-to-heating efficiency, and TEE of the system dropped from 29%, 30%, 92%, and 151% to 7%, 8%, 91%, and 105%, respectively. Li et al. [45] investigated the effects of different compressor operation modes (sliding pressure and constant pressure) and gas storage chambers (constant temperature and constant wall temperature), and compared the thermodynamic and economic characteristics under four different combinations of compressor operation conditions and gas storage chambers. The results showed that the system adopting sliding pressure operation and constant temperature gas storage chamber achieved the highest exergy efficiency of 57% and a maximum annual profit margin of 48%, while the system with constant pressure operation and a constant temperature gas storage chamber had the highest energy density of 12 MJ/m³.

Han et al. [57,58] analyzed the effects of constant pressure and sliding pressure operating modes of both the compressor and expander, and found that both RTE, TEE, and exergy efficiency were the highest, at 48%, 91% and 56%, respectively, when both the compressor and expander operated in sliding pressure mode. Further analysis of the operating modes of the expanders during discharging revealed that the system achieved optimal

performance [59], with an RTE of 41%, when one of the expander operated in constant pressure mode and the other in sliding pressure mode. Han et al. [60] also investigated the effect of the heat distribution ratio (defined as the proportion of heat in the thermal tank allocated to heating the compressed air entering the expander) on system performance. They found that the exergy efficiency and annual profit rate were higher, reaching 62% and 20%, respectively, when the heat distribution ratio was zero. Conversely, the RTE was highest at 55% when the heat distribution ratio was set to one.

He et al. [61] developed a dynamic model of the basic CAES-based CCHP system to capture the dynamic characteristics and charging strategies, including variable charging methods like constant-pressure mode with an expansion valve downstream of the compressor and sliding-pressure mode with a direct connection between the compressor and air storage tank. Their findings show that the exergy efficiency of the sliding-pressure charging mode is 3.9% higher than that of the constant-pressure charging mode. In addition, matching load with system output remains a critical challenge in practical applications. Zheng et al. [62] investigated the cooling, heating, and electric load of a typical residential area, and analyzed the characteristics of a basic CAES-based CCHP system for trigeneration in different seasons. By matching the load and the trigeneration features, they defined an optimal heat distribution ratio to determine the proportion of cooling, heating and power generation and the optimal heat distribution ratio for each season: 36% for summer, 94% for spring/autumn, and 36% for winter to meet the demands. The economic analysis revealed that the annual energy supply cost with the basic CAES-based CCHP system was 24% lower than that of the traditional method (supplied by coal boilers, air conditioners, and the electric grid). The annual energy cost decreased from \$1.0 million to \$0.8 million, with a *SPP* of 15.4 years.

2.2 CAES hybrid CCHP system

Certain heating and cooling components, such as absorption refrigeration systems (ARSs), absorption heat pumps (AHPs), ejector refrigeration cycles (ERCs) and organic Rankine cycles (ORCs), can be integrated into the CAES systems to form hybrid CAES-CCHP systems, to achieve better performance or meet specific demands, such as large heating or cooling needs.

For locations with large cooling demand and grid-connected renewable power plants, Arabkoohsar and Andresen [63] proposed a CAES-ARS hybrid CCHP system composed of a CAES system and a solar-powered ARS, as shown in Fig. 3. In this system, the ARS produced a considerable portion of cooling by absorbing solar thermal heat and the compression heat from the CAES during charging. The remaining cooling was

produced by the expansion devices during discharging. A case study of a hospital in Denmark, with an annual cooling demand of 3.2 MW and cooling temperature of 8 °C, was conducted. Performance analysis showed that the hybrid system reliably integrated cooling and electricity, achieving a *LCOE* of 76 \$/MWh.

Additionally, Chen et al. [64] investigated the off-design characteristics and techno-economic performance of a CAES-ARS hybrid CCHP system, as shown in Fig. 4, taking real wind fluctuation into account. With objectives focused on RTE, heating efficiency, cooling efficiency, and economic performance, the authors proposed a bi-level differential evolution algorithm for multi-objective optimization of the system, and found that decreasing the compressor load led to an increase of 20% in heating efficiency but a decrease of 5% in RTE. Conversely, reducing the expander load resulted in a decrease of 22% in cooling efficiency. Furthermore, the system achieved a maximum value of 111% in overall efficiency, with the lowest total daily costs, which consist of capital, energy, and operation costs, being \$3900, \$3700, and \$3100 in winter, summer, and transition conditions, respectively.

ERC is also a viable option for recycling waste heat for cooling [65]. Liu et al. [66] developed a CAES-ERC hybrid CCHP system for end-users in isolated lands and

seaside areas, as shown in Fig. 5, which combined an underwater CAES subsystem with an ERC subsystem. The underwater CAES, utilizing hydrostatic pressure, operated as an isobaric CAES, which prevented pressure fluctuations and ensured stable operation. In this system, the ERC was deployed downstream of the turbine to recover the exhausted waste heat from the turbine for cooling (at 10 °C), while the low-grade compression heat was used for heating (at 45 °C). A multi-objective optimization was conducted to maximize the overall exergy efficiency and minimize capital cost, with an optimized design delivering an overall exergy efficiency of 56% and a capital investment cost of \$334000.

Furthermore, Rahbari et al. [67] integrated an ORC into the CAES system to form a CAES-AHP hybrid CCHP system, as shown in Fig. 6. In this system, the ORC recovered compression heat to generate electricity, partially offsetting the power consumption of the compressors, and the waste heat from the ORC was then utilized for heating (at 80 °C), while the cooling (at 8 °C) was produced through expansion during discharging. Since air was not preheated before the expansion process, a large amount of cooling was generated, although this led to a reduction in power generation. The authors evaluated the effect of wind power fluctuations on system performance, revealing that the TEE decreased from

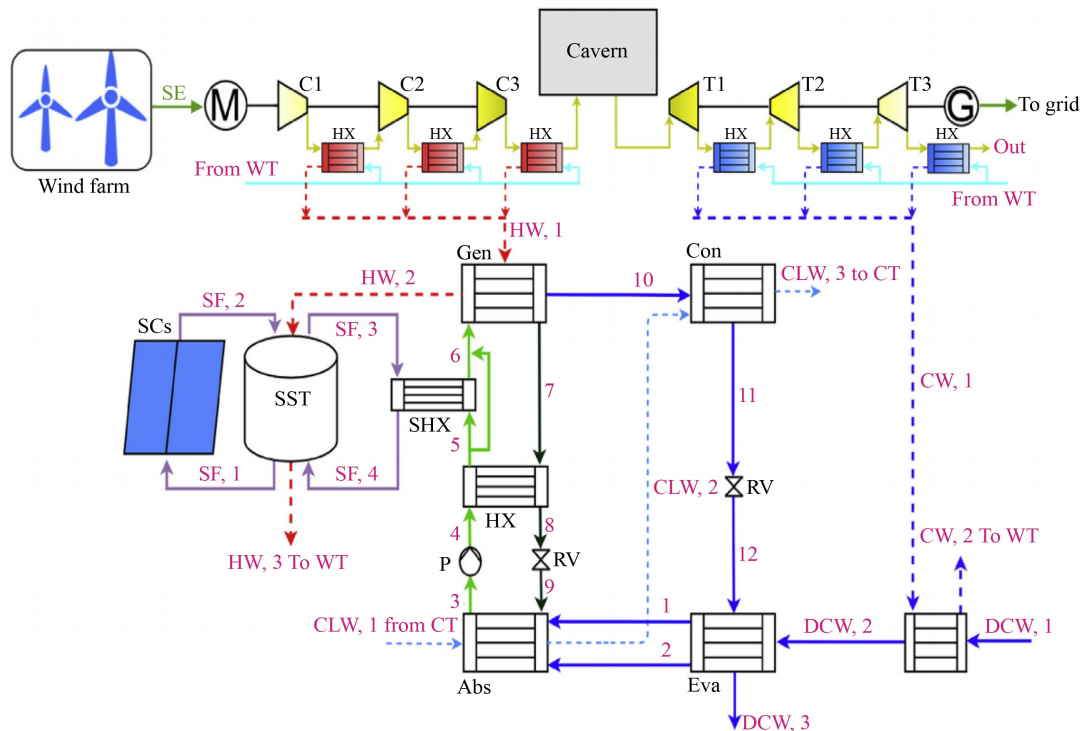


Fig. 3 Schematic diagram of the CAES-ARS hybrid CCHP system (SE: surplus electricity; M: motor; C: compressor; T: expander; HX: heat exchanger; G: electricity generator; HW: hot water; CW: cold water; yellow line: compressed air; light blue line: cooling/heating fluid in ambient temperature; dark blue line: subcooled working fluid; red line: hot working fluid; Abs: absorber; P: pump; RV: restrictor valve; HX: heat exchanger; SHX: solar heat exchanger; SST: solar storage tank; SCs: solar collectors; SF: solar system working fluid; Gen: chiller generator; Con: condenser; Eva: evaporator; CLW: cooling water; CT: cooling tower; DCW: district cooling water) (adapted from Arabkoohsar and Andresen [63], copyright 2018, Elsevier).

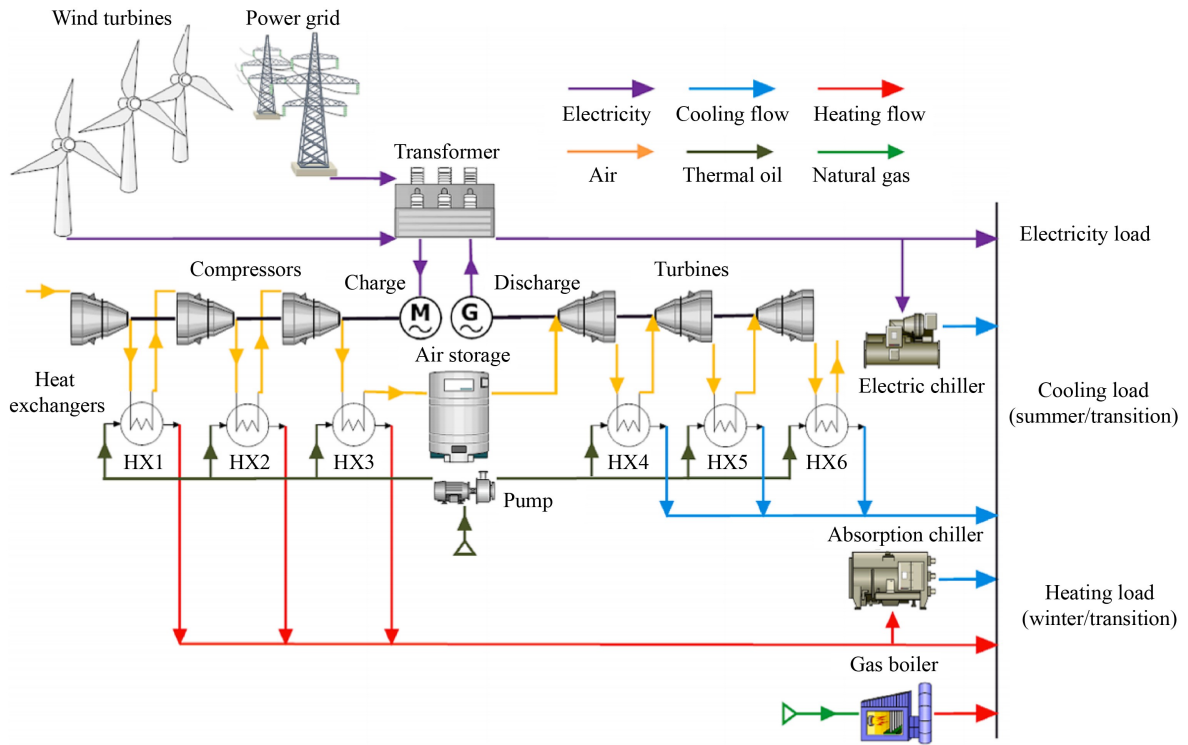


Fig. 4 Schematic diagram of the CAES-ARS hybrid CCHP system (adapted with permission from Chen et al. [64], copyright 2021, Elsevier).

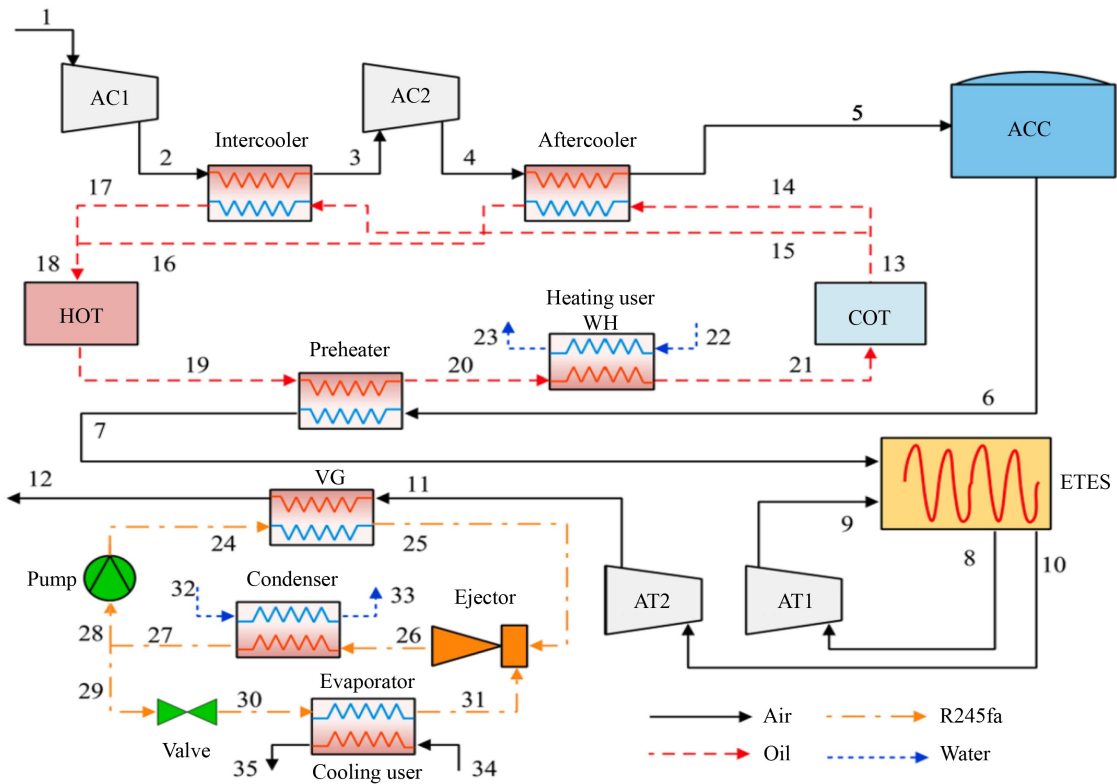


Fig. 5 Schematic diagram of the CAES-ERC hybrid CCHP system (AC: air compressor; ACC: air accumulator; AT: air turbine; COT: cold oil tank; ETES: electrical thermal energy storage; HOT: hot oil tank; VG: vapor generator; WH: water heater) (adapted with permission from Liu et al. [66], copyright 2021, Elsevier).

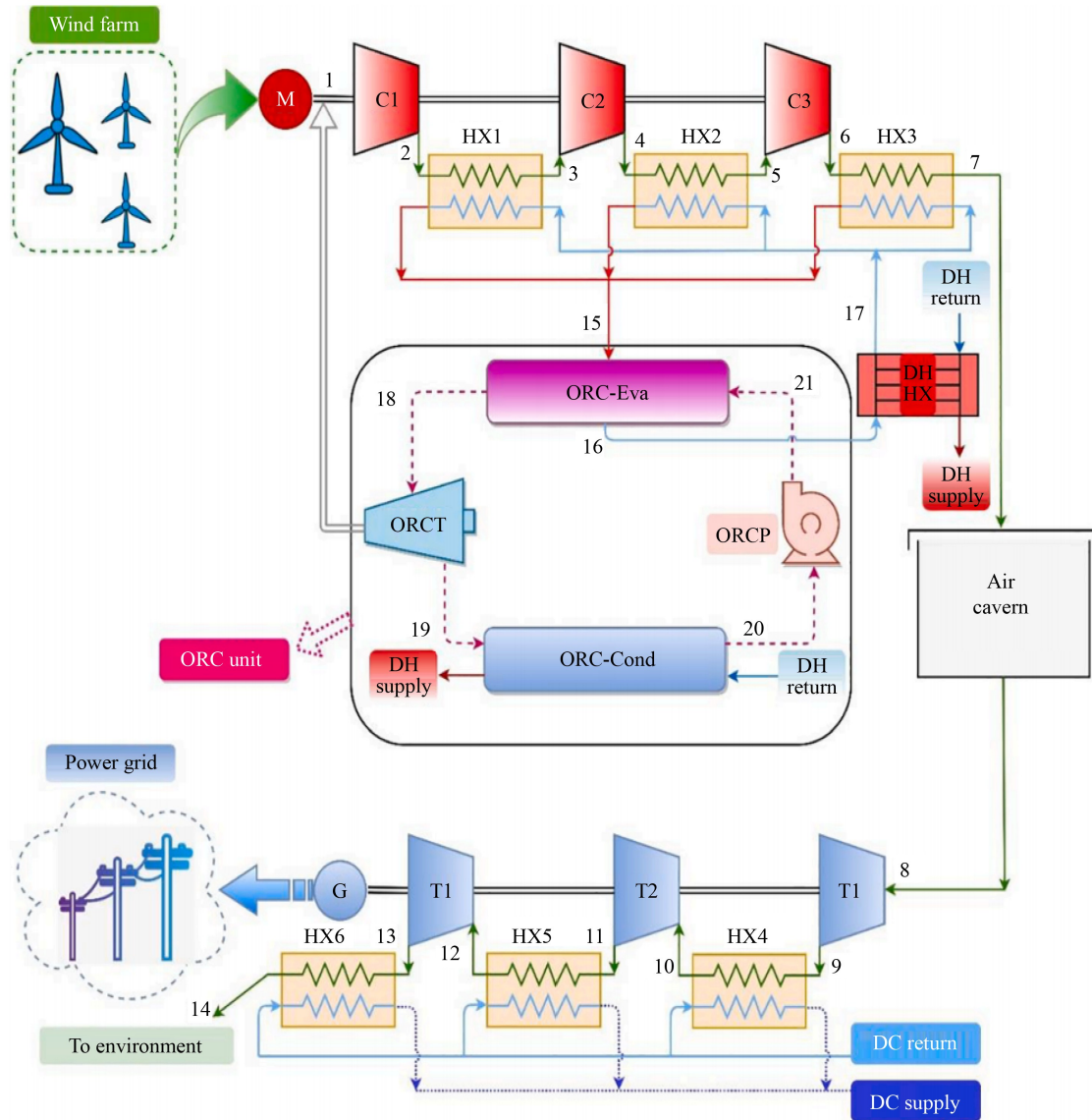


Fig. 6 Schematic diagram of the CAES-ORC hybrid CCHP system (C: compressor; T: expander; DC: district cooling; DH: district heating; Cond: condenser; Eva: evaporator) (adapted with permission from Rahbari et al. [67], copyright 2021, Elsevier).

150% in nominal mode to 126% in off-design mode. Additionally, the exergy efficiency dropped from 64% to 58%, the *LCOE* increased from 163 to 178 \$/MWh, and the potential (equivalent) carbon emissions reduction decreased from 4160 to 3640 $t_{CO_2-eq}/year$.

For regions with large heating demands, AHP can be integrated with CAES systems to increase heat capacity. Liu et al. [68] proposed a CAES-AHP hybrid CCHP system, as shown in Fig. 7. In this system, high-temperature thermal oil was split into two flows during discharging. One flow was sent to the heaters to transfer heat to the air for improving turbine power production, while the other flow drove the AHP to provide heating (60 °C) for users. The cooling energy was directly provided by the cryogenic air at the turbine outlet (−19 °C). When compared to a CAES system without

AHP, the proposed CCHP system shows improvements of 44% in heating energy, 16% in RTE, and 2.8% in exergy efficiency, with the heating power increased from 191 to 275 kW.

Ding et al. [69] and Liu et al. [70] integrated ORC and ARS into the CAES system to form a CAES-ORC-ARS hybrid CCHP system, as shown in Fig. 8. In this system, two ORCs were deployed, one during charging to offset part of compressor's power consumption, and the other during discharging to increase power generation. The waste heat from the exhaust of the turbine during discharging was split into two parts. One part was used to drive an ORC, while the other was used to drive an ARS to generate cooling. The authors optimized the key parameters of this system based on both thermodynamic and economic performances, and found that the RTE

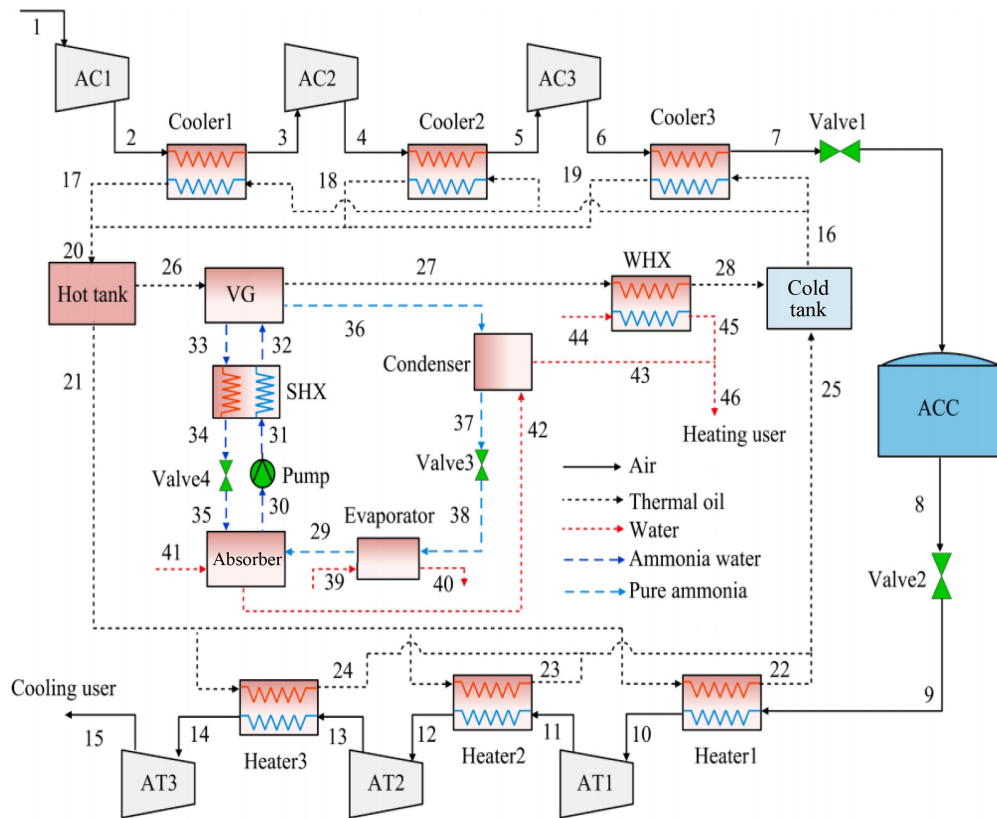


Fig. 7 Schematic diagram of the CAES-AHP hybrid CCHP system (AC: air compressor; ACC: air accumulator; AT: air turbine; WHX: waste heat recovery heat exchanger; SHX: solution heat exchanger, VG: vapor generator) (adapted with permission from Liu et al. [68], copyright 2021, Elsevier).

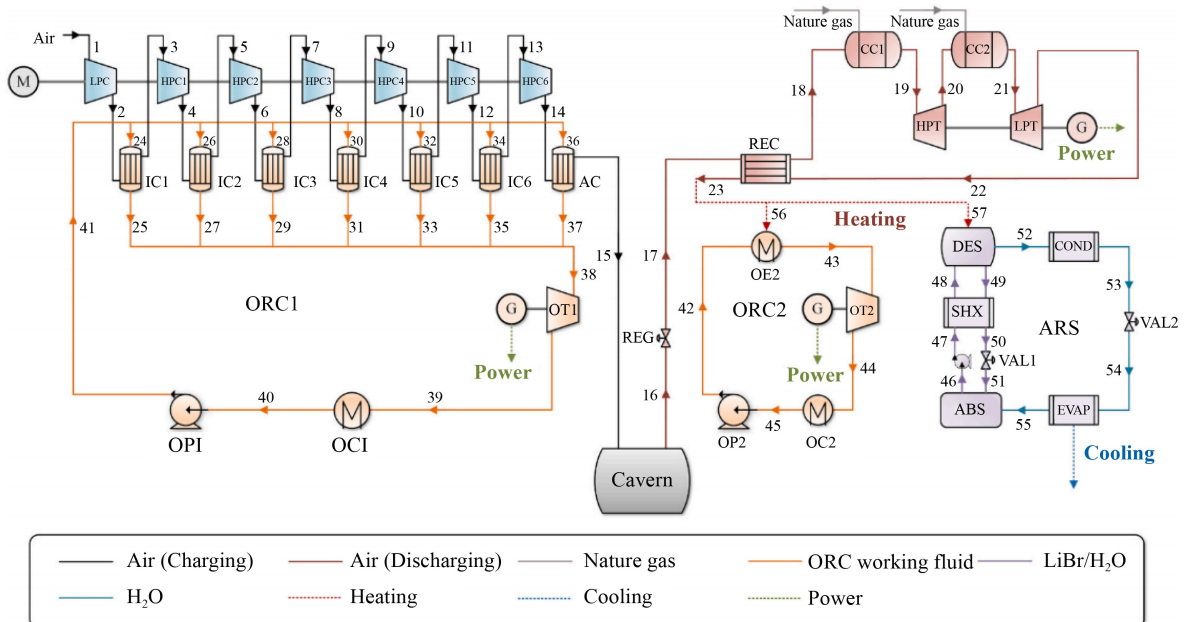


Fig. 8 Schematic diagram of the CAES-ORC-ARS hybrid CCHP system (ABS: absorber; CC: combustion chamber; COND: ARS condenser; DES: ARS desorber; EVAP: ARS evaporator; HPT: high-pressure turbine; HPC: high-pressure compressor; IC: intercooler; LPT: low-pressure turbine; LPC: low-pressure compressor; OT: ORC turbine; OC: ORC condenser; OP: ORC pump; OE: ORC evaporator; PUMP: ARS pump; REG: regulating valve; REC: recuperator; SHX: ARS solution heat exchanger; VAL: ARS valve) (adapted with permission from Liu et al. [70], copyright 2022, Elsevier).

could reach 68%, and the minimum total investment cost per output power was 194 \$/MWh. However, since the compression heat was consumed during charging, fuel was still required to heat the air at the expander inlet during discharging, warranting further assessment of the system's environmental impact.

Moreover, research on artificial intelligence (AI) applications in CAES-based CCHP systems has been gradually advancing. Assareh and Ghafouri [71] optimized the performance of a CAES-based CCHP system by integrating multi-layer perceptron architectures of artificial neural networks (ANNs) with NSGA-II multi-objective optimization algorithm. The optimized system achieved an exergy efficiency of 29% and a minimum cost rate of 714 \$/h. Subsequently, a parametric sensitivity analysis using ANNs on a solar-CAES hybrid CHP system identified five critical decision variables: the number of PV panels, CAES pressure ratio, CAES inlet pressure, gas turbine efficiency, and compressor efficiency, achieving an available energy efficiency of 36% and a cost rate of 14 \$/h [72]. Furthermore, Yun et al. [73] applied machine learning

techniques to predict and optimize a CAES-solid oxide fuel cell hybrid CCHP system. The results showed that the developed machine learning algorithms demonstrated high accuracy, and the TEE and the exergy efficiency of the system could reach 63% and 33%, respectively. The current findings support AI's potential in identifying key variables and their intercorrelations in CCHP systems. However, there remains a gap in research on AI-driven control strategies for CAES-based CCHP systems that can flexibly respond to various energy demands.

An overview of the performance metrics of CAES-based CCHP systems is summarized in Table 1. CAES, as the most mature TMES technology, has driven further exploration of its application in CCHP systems, particularly in adiabatic CAES configurations. Based on the aforementioned research, the RTE of CAES-based CCHP systems ranges from 23% and 68%, while the TEE varies from 65% to 155%. These CCHP systems offer significant economic benefits over traditional CCHP systems, with a reduction in annual energy supply costs by approximately 20%.

Table 1 Performance metrics of CAES-based CCHP systems

Type	Refs.	RET/%	TEE/%	Exergy efficiency/%	Heating temperature/°C	Cooling temperature/°C	Economic indicators	Scale
Basic CAES-based CCHP	Lv et al. [43]	–	76	–	–	–	Annual reduced operating cost: 54%	–
	Facci et al. [52]	30	–	46	53 to 89	–3 to 5	–	150 kW
	Kim et al. [51]	–	–	74	80	–6	–	10 kW
	Li et al. [53]	35 to 50	–	–	–	–	–	100 kW
	Arabkoohsar et al. [50]	31	155	48	60	8	Annual benefit: \$9200000	300 MW
	Alsagri et al. [56]	29	150	–	80	8	–	–
	Wang et al. [55]	54	101	–	80	–	–	5 MW Charge/discharge period: 5 h
	Li et al. [45]	–	–	57	260	–25	Annual profit margins: 16%–48%	120 MW
	Han et al. [57, 58]	48	91	57	200	–37	Annual profit margins: 15%–30%	100 MW Charge/discharge period: 4 h
	Li et al. [74]	–	–	54	170	–	–	100 MW Charge/discharge period: 4 h
	Jiang et al. [75]	54	76	–	–	–	Annual total cost saving: 194000 \$	830 kW 5 MWh 300 MWh
	Li et al. [76]	62	96	–	60	–	–	Charge/discharge period: 7 h
	He et al. [61]	–	128	66	52 to 96	–15 to 16	SPP: ~4 years	–
	Zheng et al. [62]	52	–	–	143	5	SPP: ~15 years	–
CAES hybrid CCHP	Arabkoohsar and Andresen [63]	–	–	–	–	8	LCOE: 76 \$/MWh	3.2 MW 300 MWh
	Sadreddini et al. [77]	–	72	–	75	–10	–	60 kW Charge/discharge period: 4 h
	Razmi et al. [78, 79]	57	65	49	–	–	SPP: ~3 years	500 kW Discharge period: 4 h
	Chen et al. [64]	23	111	–	–	–	Total daily cost: \$3100 to \$3900	–
	Liu et al. [66]	54	77	56	45	10	Capital investment cost: \$334000	500 kW Charge/discharge period: 6 h
	Rahbari et al. [67]	–	150	64	80	8	LCOE: 163 \$/MWh	5 MW Charge/discharge period: 12 h
	Liu et al. [68]	56	120	63	60	–19	–	500 kW
Liu et al. [70]	68	–	–	–	–	LCOE: 194 \$/MWh	200 MW Charge/discharge period: 3 h	

3 LAES for CCHP

3.1 Basic LAES-based CCHP system

In contrast to CAES systems, LAES systems store liquid air rather than compressed air, which mainly consist of compressors, expanders, liquid air storage tanks, cold boxes, separators, heat exchangers and thermal energy storage, as shown in Fig. 9. During charging, the air is compressed, cooled, expanded, and liquefied, then stored in liquid air storage tanks at approximately 78 K and near-ambient pressure. The compression heat generated during this process is either stored in a heat store or used for subsequent heating. During discharging, the stored liquid air is first pumped to high pressure, releasing high-grade cold energy, which is stored in the cold store for reuse during liquefaction. Subsequently, the high-pressure air is heated by environmental heat and superheated using stored compression heat before being sent to the expander to generate electricity. Part of the heat and cold energy stored in the heat store and cold store can be selectively extracted for heating and cooling, as indicated by the red and blue dotted lines in Fig. 9. Such CCHP systems, consisting solely of basic LAES systems, are referred to as basic LAES-based CCHP systems.

The temperature of stored compression heat ranges from 350 to 160 °C, while the temperature of the stored cold reaches -194 °C. Although such basic LAES-based CCHP systems can deliver heat and cold within these temperature ranges, current studies primarily focus on district heating (between 50 and 70 °C) and district cooling (between 0 and 10 °C). For example, such basic LAES-based CCHP systems can provide 20–47 MWh of power, 9–50 MWh of heating, and 8–12 MWh of cooling, with 100 MWh of input power, achieving an NRTE ranging from 47% to 73% [80]. Another cooling

method involves limiting the air temperature at the expander inlet during discharging (usually below 100 °C) to ensure that the outlet temperature meets the cooling demand, as shown by the blue dotted line 2 in Fig. 9. However, this cooling method reduces the enthalpy drop during expansion, resulting in an 8% reduction in RTE [44].

Heating and cooling have distinct effects on basic LAES-based CCHP systems. Heating only affects the charging process, while cooling affects both the charging and discharging process. When the system is used exclusively for power generation, approximately 20%–45% of the compression heat is surplus [81], meaning that this heat can be utilized for heating without significantly compromising power generation efficiency. However, higher heating output reduces the expander inlet temperature, which in turn decreases power generation but does not affect cooling capacity. A 10% increase in the amount of heat consumed for heating leads to a maximum 7% reduction in NRTE [80].

For higher cooling output, both the required electricity during charging and the produced compression heat increase, as more air must be compressed and liquefied. An increase of 10% in the amount of cold consumed for cooling results in a reduction of up to a 14% in NRTE [80]. Therefore, basic LAES-based CCHP systems are more suitable for combined heating and power applications.

Although providing large amounts of heating and cooling reduces power generation, this decrease can be offset by the technical and economic advantages. The highest economic benefits are achieved by maximizing the combined supply of heat and electricity, as this maintains high electrical efficiency and fully exploits the available compression heat. In one case study, the operating costs of LAES-based CCHP systems were expected to decrease by 13%, compared to the operating

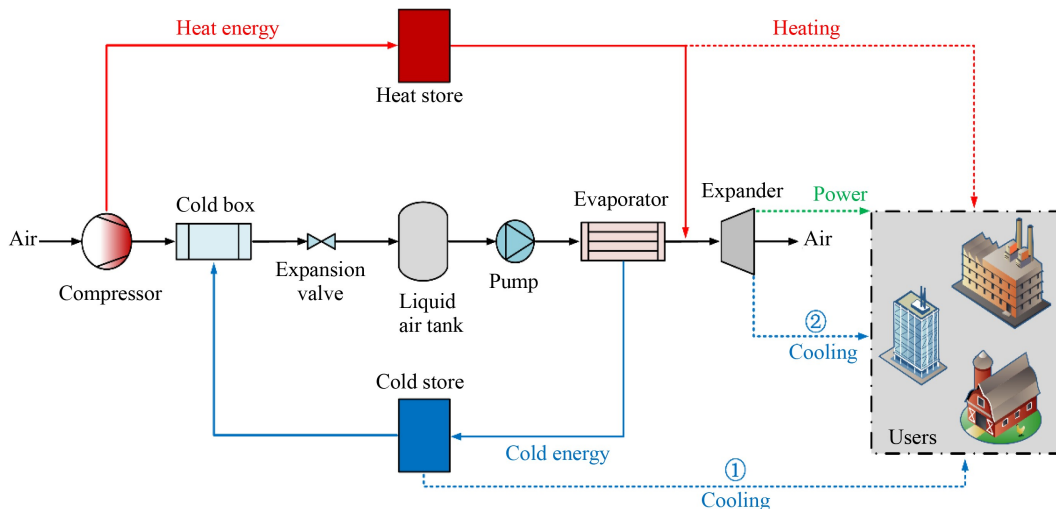


Fig. 9 Schematic diagram of basic LAES-based CCHP system.

1870 GJ of electricity, 58 GJ of cooling energy, and 120 GJ of heating annually, with an NRTE of 67% and a carbon emission reduction of 368 tons, and the dynamic payback period was 6.5 years.

In addition to integrating with ARS, Tafone et al. [44] introduced both ORC and ARS to the basic LAES system to form a LAES-ARS-ORC hybrid CCHP system, as shown in Fig. 11. In this CCHP system, part of the stored compression heat was first used to power the ORC to improve power generation efficiency. Then, the ARS was driven by the waste heat discharged by the ORC at a temperature of 105 °C, and generated chilled water at a temperature of 6 °C for air conditioning applications, while the waste heat from the ARS was used for heating at a temperature of 52 °C. The RTE and NRTE of the LAES-ARS-ORC hybrid CCHP system were found to be 13% and 6% higher than those of the basic LAES CCHP system, respectively, due to better utilization of the available waste heat.

Further analysis by Xue et al. [84] involved constructing a mathematical model of the LAES-ARS-ORC hybrid CCHP system, based on the first and second laws of thermodynamics and analyzed the exergy characteristics of key components. It was found that the exergy loss of ARS and ORC was relatively small compared to that of the LAES system, and the largest exergy loss occurred during the processes of air liquefaction, throttling, and regasification in the compressed air.

To fully optimize the performance of waste heat utilization equipment, Li and Duan [85] designed a solar-

aided LAES-ARS-ORC hybrid CCHP system, as shown in Fig. 12. In this system, the ORC subsystem operated in both the charging and discharging processes, achieving the dual-purpose functionality of “one machine with two uses”. During charging, the ORC used compression heat to generate electricity, offsetting part of the power consumption of the air compressor. During discharging, the ORC used low-temperature waste heat to generate electricity, while also transport lower-temperature WF to the ARS. The ARS, in turn, provides heating at 78 °C and cooling at -1 °C for supply. The system achieved an exergy efficiency of 51%, with an output of 11.7 MW of power, 241 kW of heat exergy, and 25 kW of cold exergy. The dual-side integration of ORC in LAES-ARS-ORC hybrid CCHP system was found to be more efficient than the single-side integration, as shown in Fig. 11, with RTE improved by 16%.

Moreover, Ding et al. [86] proposed a LAES-ARS hybrid CCHP system integrated with solar thermal and hydrogen production capabilities. This system could generate 59 MW of electricity, 27 MW of cooling energy, 35 MW of heating energy, 67.94 kg/s of domestic hot water, and 12.17 mol/s of hydrogen. Compared to traditional LAES systems, this hybrid CCHP system improved the TEE by 21%, but reduced the exergy efficiency by 15%.

The various configurations of LAES hybrid CCHP systems, which incorporate ARS and/or ORC into the basic LAES-based CCHP system, are summarized in Fig. 13. There are two main configurations for the LAES-

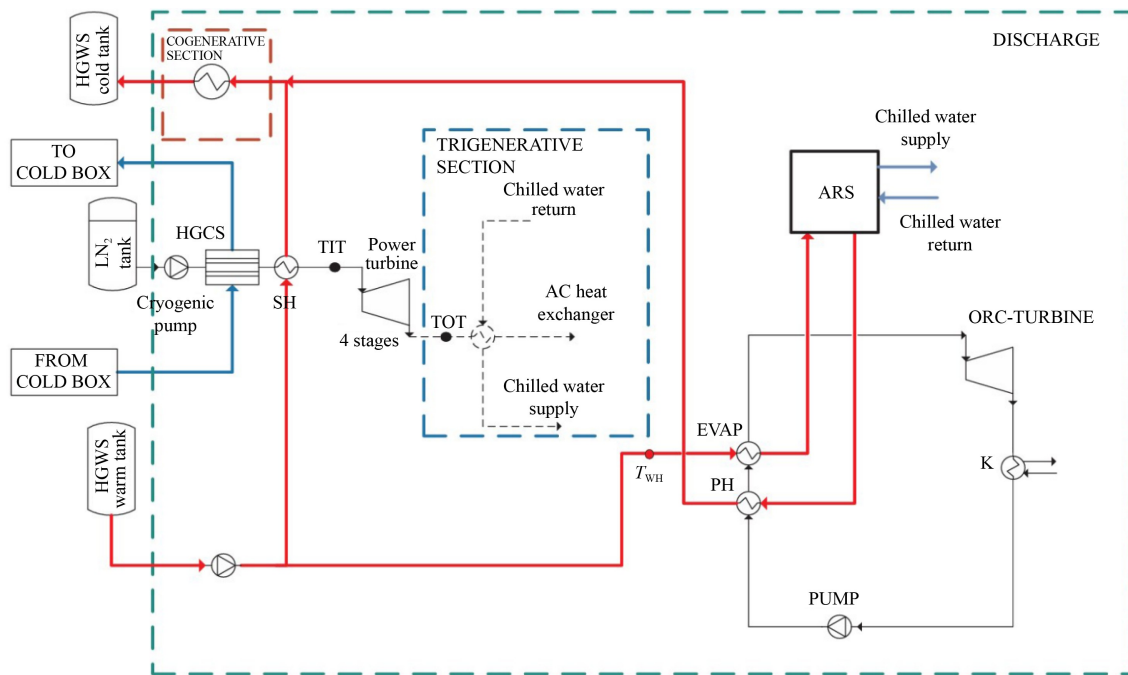


Fig. 11 Schematic diagram of the LAES-ARS-ORC hybrid CCHP system (AC: air conditioning; ORC evaporator; HGCS: high-grade cold storage; HGWS: high-grade warm storage; IC: intercooler; K: ORC condenser; PH: preheater) (adapted with permission from Tafone et al. [44], copyright 2018, Elsevier).

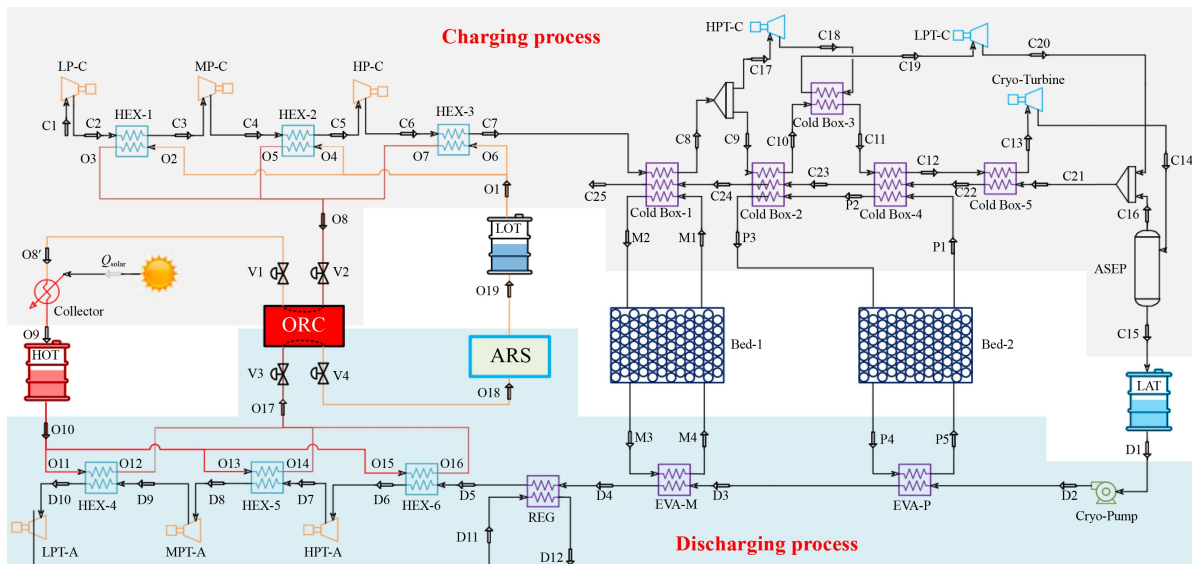


Fig. 12 Schematic diagram of the LAES-ARS-ORC hybrid CCHP system (ASEP: air separator; EVA: evaporator; HEX: heat exchanger; HOT: high-temperature thermal oil tank; HP-C: high-pressure compressor; HPT-A: high-pressure air turbine; HPT-C: Claude cycle high-pressure turbine; LAT: liquid air tank; LOT: low-temperature thermal oil tank; RC: ORC condenser; RE: ORC evaporator; REG: regenerator; RP: ORC pump; RT: ORC turbine) (adapted with permission from Li and Duan [85], copyright 2022, Elsevier).

ARS hybrid CCHP systems, depending on whether the ARS is deployed in discharging process or charging process. In the configuration shown in Fig. 13(a), ARS is deployed during the discharging process, utilizing stored compression heat to generate both heating and cooling. In Fig. 13(b), ARS is deployed during the charging process, using compression heat generated during charging to produce heat and cold energy for the air liquefaction process, thereby reducing power consumption. In this configuration, cooling is provided by the expander.

The LAES-ORC hybrid CCHP system is shown in Fig. 13(c), where ORC is deployed in the discharging process to use stored compression heat for power generation. In the LAES-ARS-ORC hybrid CCHP systems shown in Fig. 13(d), both ORC and ARC are deployed in the discharging process, with ARC using waste heat from ORC to generate heating and cooling. Additionally, as shown in Fig. 13(e), ORC can also be deployed in the charging process, where it utilizes compression heat to generate electricity, offsetting part of the compressor power consumption. The ORC in the charging and discharging processes may be identical, as depicted in the system in Fig. 12.

Among these LAES hybrid CCHP systems, the LAES-ARS-ORC hybrid CCHP systems, shown in Fig. 13(e), exhibit the highest RTE and TEE. However, these systems are the most complex and may encounter unforeseen challenges in terms of operation and cost. The LAES-ARS-ORC hybrid CCHP systems depicted in Fig. 13(d) outperform the LAES-ARS hybrid CCHP systems shown in Fig. 13(a), but they are more costly. Therefore, a detailed techno-economic evaluation is necessary for their practical application. The LAES

hybrid CCHP systems, as shown in Figs. 13(b) and 13(c), rely on the expander for cooling, which limits the expander inlet temperature and consequently leads to poor thermodynamic performance.

An overview of the performance metrics of LAES-based CCHP systems is summarized in Table 2. LAES systems typically incorporate ORC and ARS to form CCHP systems, with RTE ranging from 40% to 91% and exergy efficiency between 50% and 61%. Compared to CAES-based CCHP systems, large-scale LAES-based CCHP systems offer the advantage of storing liquid air without the need for underground caverns, thus avoiding geographical constraints. However, further exploration is needed to integrate these LAES hybrid CCHP systems with various renewable energy sources and loads. Moreover, optimizing the allocation of heat and cold for power generation, heating, and cooling is crucial to reduce investment and operating costs, ultimately improving the effective design of these systems.

4 Pumped-thermal energy storage for CCHP

4.1 ORC-PTES-based CCHP

Basic ORC-PTES systems typically consist of compressors, expanders, evaporators, condensers, and thermal energy storage, as depicted in Fig. 14, which generally use refrigerants as WF, such as butene, R1233zd(E), toluene, cyclopentane, n-pentane, and n-heptane, [37], although ORCs using water as a WF have also been reported [89]. The basic operating principle is

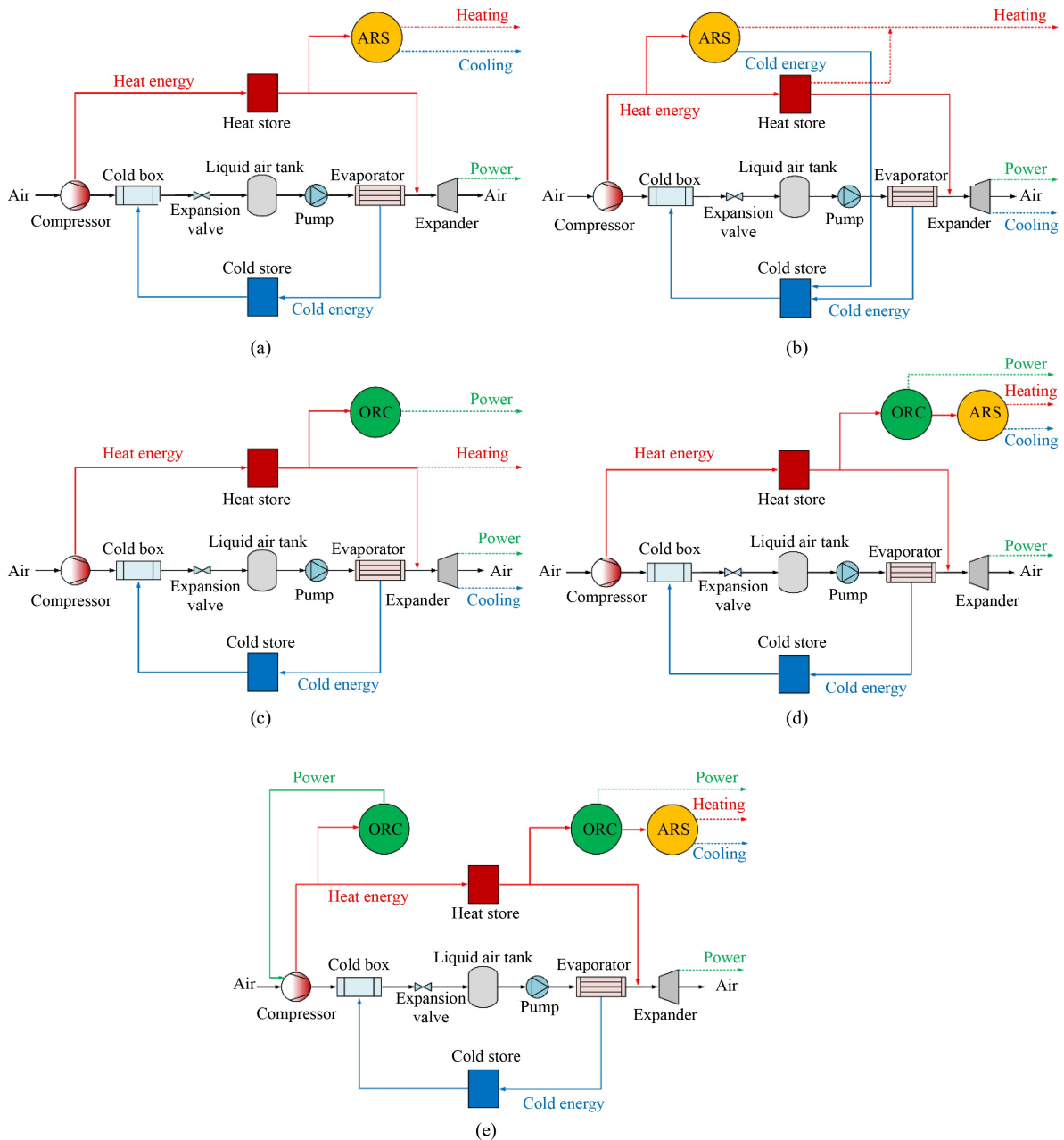


Fig. 13 Schematic diagram of LAES hybrid CCHP system configurations.

(a) LAES-ARS-1 hybrid CCHP systems; (b) LAES-ARS-2 hybrid CCHP systems; (c) LAES-ORC hybrid CCHP systems; (d) LAES-ARS-ORC-1 hybrid CCHP systems; (e) LAES-ARS-ORC-2 hybrid CCHP systems.

as follows: during charging, the WF absorbs external heat in the evaporator, and is then compressed to a pressurized, higher-temperature state, converting electricity into heat. This heat is stored in the heat store, and subsequently, the WF expands back to its initial state via the expansion valve. During discharging, the WF is first pumped to the heat store to absorb heat, then expands in the expander, driving the generator to produce electricity. Finally, it ejects waste heat in the condenser and returns to its initial state.

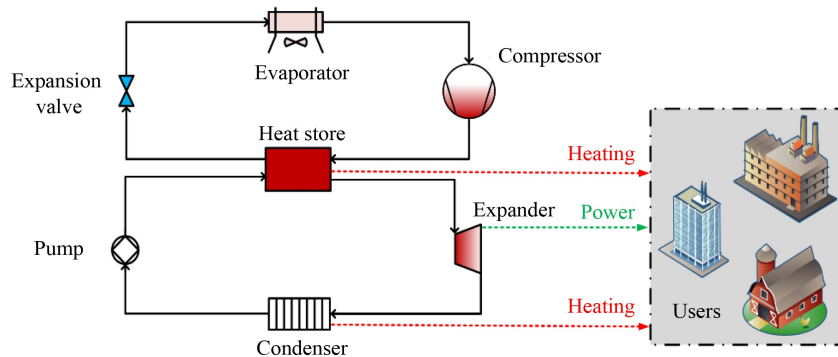
These ORC-PTES systems can also function as

combined heating and power (CHP) systems by utilizing the thermal energy stored in the heat store during charging and/or heat rejected at the condenser during discharging for heating purposes [90]. However, due to the critical temperature of the WF (refrigerant), the operating temperature of these systems typically remains below 200 °C, which also limits the heating temperature to below 200 °C.

One advantage of ORC-PTES systems is their ability to convert low-grade external heat sources, such as solar heat, geothermal energy, and industrial waste heat, into

Table 2 Performance metrics overview of LAES-based CCHP systems

Type	Refs.	RET/%	TEE/%	NRTE/%	Exergy efficiency/%	Heating temperature/°C	Cooling temperature/°C	Economic indicators	Scale
Basic LAES-based CCHP	Vecchi et al. [80]	–	73	–	–	60 to 120	–	Reduced operating cost: 8% to 12% DPP: < 20 years	5 to 80 MW 20 to 300 MWh 10 MW
	Jenkins [47]. and Tafone et al. [87]	40 to 70	–	45 to 50	–	115	5	–	10 MW
LAES hybrid CCHP	Tafone et al. [44]	53	–	56	–	41 to 57	6 to 8	–	10 MW
	She et al. [82]	–	–	76	–	55 to 85	7	SPP: ~3 years	5 MW 40 MWh Charge/discharge period: 8 h
	Wang et al. [88]	39	–	–	59	–	–	SPP: ~6 years	10 MW 80 MWh 5 MW
	Gao et al. [46]	46	–	55	50	60	7	LCOE: 174 \$/MWh DPP: ~6 years	Charge/discharge period: 8 h 500 MWh
	Chen et al. [83]	–	–	67	–	60	7	LCOE: 96 \$/MWh DPP: ~7 years SPP: ~5 years	–
	Xue et al. [84]	56	70	–	57	60	7	–	10 MW
	Li and Duan [85]	91	–	–	51	78	–1	–	1 MW Charge/discharge period: 6 h
	Esmailion et al. [17] Ding et al. [86]	53 51	64 72	– –	61 36	– –	– –	SPP: ~3 years LCOE: 90 \$/MWh DPP: ~4 years	10 MW Charge/discharge period: 8 h/4 h 100 MW

**Fig. 14** Schematic diagram of ORC-PTES-based CHP system.

higher-grade heat through a heat pump cycle, thereby enhancing both the RTE and TEE. Additionally, the RTE improves significantly with an increase in the waste heat source temperature. For instance, when the temperature of the waste heat source increases from 40 to 100 °C, the RTE improves from 46% to 130% [91, 92].

However, if ORC-PTES systems are specifically designed, the evaporator can provide cooling, leading to the formation of CCHP systems, as shown in Fig. 15, which employ a multi-stage heat pump. The first stage produces cooling at approximately 0 °C via Evaporator 1, while the second stage generates heat at around 50 °C, which is stored in Heat store 1 for potential use of space heating. Evaporator 2 operates near ambient temperature. This is achieved by two parallel evaporators (Evaporator 1 and Evaporator 2) operating at different pressures. In the third stage, heat from Heat store 1 is utilized to produce high-temperature heat (approximately 115 °C), which is then stored in Heat store 2 for power generation through an ORC system [93].

In such ORC-PTES CCHP systems, an increase in the cooling load at 0 °C results in a reduction in power

generation and decreased heat absorption from the environment, while simultaneously leading to higher power consumption [93]. Similarly, an increase in the heating load at 50 °C diminishes power generation, but enhances heat absorption from the environment and increases power consumption. A case study showed that such ORC-PTES CCHP systems could achieve an exergy efficiency of 50%. When operating 2000 h per year, the SPP of the system was approximately 2.5 years, with a total annual equivalent carbon emission avoidance of 45.6 t_{CO₂-eq} per year in terms of environmental benefits [93]. However, distribution of exergy loss within the ORC-PTES CCHP systems remains unexplored, and further thermodynamic optimization of the system for heating and cooling is needed.

Additionally, Chen et al. [94] proposed an ORC-PTES CCHP system coupled with solar photovoltaic-thermal (PVT) collectors. They found that integration of PVT increased the RTE by 12% compared to the system without PVT. However, due to the system's complexity, the LCOE reached 533 \$/kWh, which was significantly higher than that of other CCHP systems.

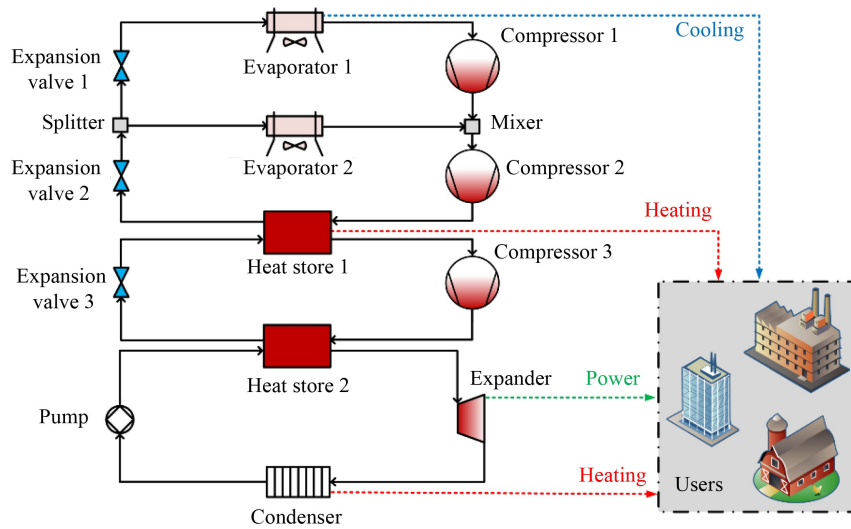


Fig. 15 Schematic diagram of ORC-PTES-based CCHP system.

4.2 Joule-Brayton PTES-based CCHP

Joule-Brayton PTES-based CCHP systems primarily consist of compressors, expanders, heat/cold stores, and heat exchangers, as shown in Fig. 16. These systems typically utilize air or an inert gas as the WF, which allows for a wider operating temperature range. This approach not only enhances the roundtrip (power to power) but also enables the systems to meet a broader range of thermal (heating and/or cooling) demands.

The basic operating principle can be summarized as follows: during charging, the WF is compressed by the compressor and then directed to the heat store, where it releases heat. Subsequently, the WF expands in the expander to a low-temperature state and flows into the cold store to release cold. Any excess cold and heat are released in the heat exchangers. During discharging, the WF first enters the cold store to absorb cold, then is compressed to a high-pressure state. It subsequently flows into the heat store to absorb heat before expanding

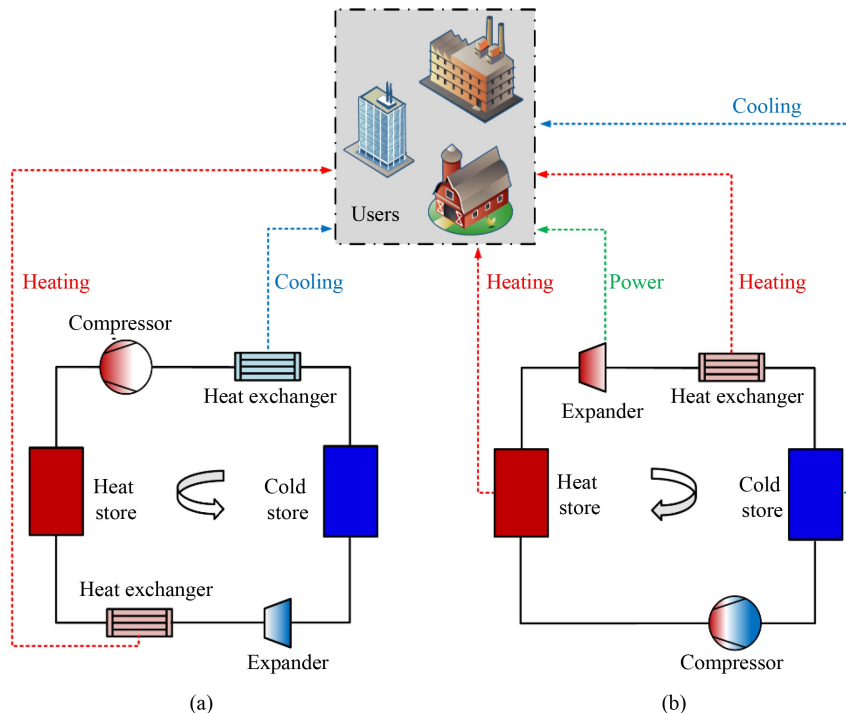


Fig. 16 Schematic diagram of Joule-Brayton PTES-based CCHP system. (a) Charge; (b) discharge.

in the expander to perform work, finally releasing waste heat in the heat exchanger. In Joule-Brayton PTES-based CCHP systems, heating and cooling can be directly extracted from the heat/cold store for respective applications. These processes can be conducted independently of power generation, offering greater operational flexibility.

For these Joule-Brayton PTES-based CCHP systems, extending the heating and cooling durations reduces the discharging duration. However, the TEE increases with the extension of the heating duration but decreases with the extension of the cooling duration, indicating that these systems are more suitable for heating from an energy perspective [95].

Compared to basic Joule-Brayton PTES systems, these Joule-Brayton PTES-based CCHP systems exhibit changes in exergy losses. Exergy losses mainly occur in compressors and expanders, accounting for about 50% of the total [95]. Additionally, exergy losses in the heat store, cold store, and heat exchangers for heating and cooling increase during heating and cooling operations. The extent of these losses depends on the grade of the supplied heat and cold. Moreover, the exergy losses of heat exchangers for heating and cooling are also influenced by the temperature difference during heat transfer. Therefore, the design and optimization of such heat exchangers require further study to improve thermodynamic performance of these systems.

It is possible for Joule-Brayton PTES-based CCHP systems to supply multi-grade heat and cold simultaneously by cascading the heat and cold stores [96,97], as shown in Fig. 17 [98]. Such Joule-Brayton PTES-based CCHP systems, incorporating cascaded latent heat and cold stores, divide the electro-transformed heat and cold into multiple grades for storage, thereby enabling a more flexible release of cold and heat across temperatures ranging from -140 to 550 °C. Furthermore, such system based on cascaded latent heat and cold stores

can be integrated with external heat and cold sources by increasing WF mass flow rate during discharging and extending the discharging duration, thereby enabling the storage and utilization of power, heat, and cold energy. A case study conducted for a large energy hub in China demonstrated that the TEE and exergy efficiency of such systems were 119.3% and 85.1%, respectively [99].

Although providing heat and cold can reduce the system's power generation efficiency, a well-balanced configuration of these heat and cold supplies, in terms of both quality and quantity, can enhance the TEE in CCHP mode. Nonetheless, determining the optimal match between the temperature and quantity of heating and cooling to improve the thermodynamic performance of CCHP systems remains an urgent issue to address.

An overview of the performance metrics for PTES-based CCHP systems is summarized in Table 3. The operational principle of PTES involves the direct conversion of electrical energy into thermal energy for storage, with the stored thermal energy available for direct output. This results in relatively straightforward configurations for PTES-based CCHP systems, particularly those employing the Joule-Brayton cycle. Such CCHP systems are capable of providing high-grade heat and cold and are not limited by geographical constraints, making them more flexible and promising. However, a comprehensive economic analysis of Joule-Brayton PTES-based CCHP systems is urgently required to assess their economic feasibility.

5 CES for CCHP

Compared to air, CO_2 has a much higher critical temperature, making it more prone to liquefaction and offering superior heat transfer characteristics [102]. As a result, CO_2 energy storage (CES) and CES-based CCHP systems have recently gained increasing attention.

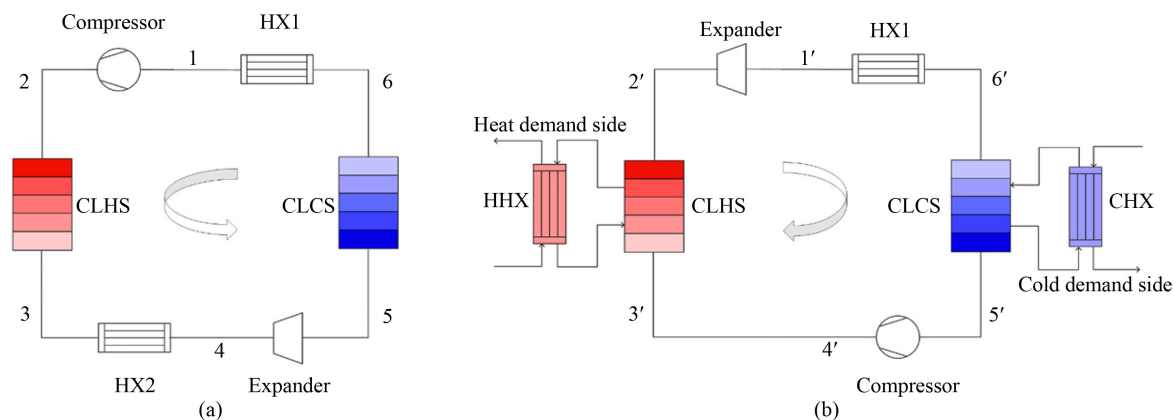


Fig. 17 Schematic diagram of Joule-Brayton PTES-based CCHP systems with cascaded latent heat and cold stores: (a) Charge; (b) discharge (HHX: heating heat exchanger; CHX: cooling heat exchanger; CLHS: cascaded latent heat store; CLCS: cascaded latent cold store) (adapted with permission from Zhao et al. [98], copyright 2024, Elsevier).

Table 3 Performance metrics overview of PTES-based CCHP systems

Type	Refs.	RET/%	TEE/%	Exergy efficiency/%	Heating temperature/ °C	Cooling temperature/ °C	Economic indicators	Scale
ORC-PTES-based CCHP	Lin et al. [89] (ORC)	57	–	–	102	–	Reduced operating cost: 29%	100 kW
	Jockenhöfer et al. [91] and Steinmann et al. [92]	125	–	59	45	–	–	1 MW
	Poletto et al. [90]	–	–	–	50 to 85	–	SPP: ~9 years	10 kW
	Lykas et al. [93]	–	–	50	50	–	SPP: 3 years	150 kW
	Chen et al. [94]	–	51	–	80	7	LCOE: 533 \$/MWh	1 MW
Joule-Brayton PTES-based CCHP	Zhang et al. [95]	64	188	64	75	7	–	10 MW
	Alsagri [100]	27	83	–	150 to 250	–	–	Charge/discharge period: 4 h 50 MW 500 MWh
	Zhao et al. [98]	58	95	52	50 to 550	–150 to 0	–	3 MW Charge/discharge period: 6 h
	Huang et al. [99]	70	120	85	50 to 550	–150 to 0	–	3 MW Charge/discharge period: 6 h
	Wang et al. [101]	–	146	63	50 to 120	–50 to 8	–	20 kW Charge/discharge period: 5 h

The CES-based CCHP systems consist of components such as compressors, expanders, high-pressure and low-pressure storage tanks, cold boxes, heat exchangers, pumps, throttling valves, thermal storage tanks, and valves, as shown in Fig. 18. The basic operating principle is as follows: during charging, liquid CO₂ from the low-pressure storage tank is transformed into a two-phase gas-liquid flow through the throttling valve, storing cold energy in the cold storage for subsequent use during discharging. Subsequently, the gaseous CO₂ is compressed by a single-stage or multi-stage compressor and stored in the high-pressure tank, either in a supercritical state or as a liquid. The heat generated during compression is recovered via an intercooler, either stored in the thermal storage tanks or directly used for heating. During discharging, the CO₂ in the high-pressure storage tank flows through the throttle valve into the intermediate heater at a stable pressure, then enters a single-stage or multi-stage expander to perform work. By adjusting the temperature and pressure of the CO₂ entering the expander, cold energy can be generated and supplied.

Similar to CAES-based CCHP systems, the heating temperatures in CES-based CCHP systems are

determined by the compression process and are inversely related to the number of compression stages, typically ranging between 50 and 250 °C. The cooling temperatures are determined by the expansion process and generally fall between –24 and 10 °C.

The performance and improvements of such CES-based CCHP systems have been extensively investigated. Liu et al. [103] presented a CES-based CCHP system, as shown in Fig. 19, where the compression heat was used for heating with temperatures ranging from 86 to 244 °C. The cryogenic CO₂ at the turbine outlet was used to produce cooling (–24 °C) via heat exchanger HE3. Different energy demands could be met by adjusting the mass flow rate of Stream 15. The authors examined the effects of key parameters on system performance, such as hot fluid reutilization ratio (HFRR, defined as the ratio of the mass flow rate of hot water used to heat supercritical CO₂ to that directly supplied to heating users), and found that decreasing HFRR improved cooling capacity, heating capacity, and total output energy, but decreased electricity generation. This indicated that such CES-based CCHP systems were much more suitable for heating applications than for cooling. The RTE, TEE and exergy

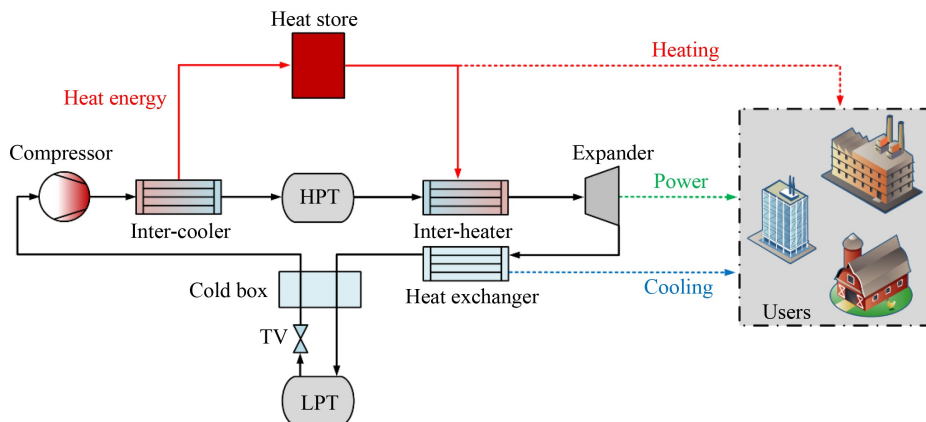


Fig. 18 Schematic diagram of basic CES-based CCHP system (HPT: high-pressure tank; LPT: low-pressure tank; TV: throttle valve).

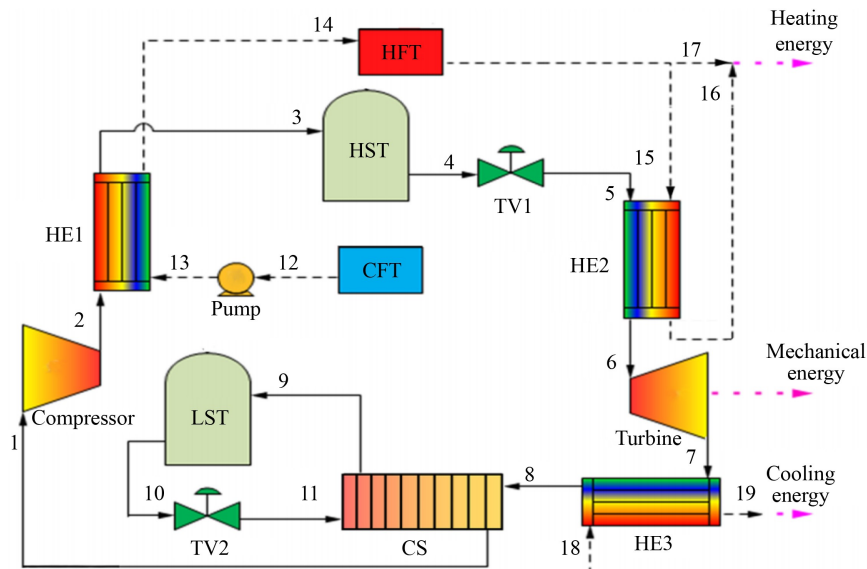


Fig. 19 Schematic diagram of the CES-based CCHP system (HE: heat exchanger; HST: high-pressure storage tank; TV: throttle valve; CS: cold storage; LST: low-pressure storage tank; CFT: cold fluid tank; HFT: hot fluid tank) (adapted with permission from Liu et al. [103], copyright 2019, Elsevier).

density of the CES-based CCHP system were 36%, 134%, and 15.0 kWh/m³, respectively, which were 12% lower, 43% higher, and four times higher than the basic CAES-based CCHP systems in Han and Guo [57].

Following this, Zhang et al. [104] applied the CES-based CCHP system to wind energy (including wind power and wind waste heat) scenarios and analyzed the effect of parameters such as the CO₂ mass flow distribution ratio, storage pressure, ambient temperature, pressure difference at the main throttle valve, and the waste heat temperature on the system performance. The authors found that the RTE and TEE of such CES-based CCHP systems were 48% and 119%, respectively, under design conditions. Compared to CAES-based CCHP systems, the proposed CES-based CCHP systems achieved 28% higher TEE while maintaining the same RTE.

To increase the cooling capacity of CES-based CCHP systems, Deng et al. [105] proposed a method where the liquid CO₂ stored in the high-pressure tank was split into two streams during discharge, one directed to the power generation branch and the other toward the cooling branch. The cooling branch was established by directly throttling liquid CO₂, allowing the system's cooling capacity to be adjusted to meet the varying energy demands of users. The authors found that this configuration significantly increased the cooling capacity and offer more flexible regulation of the cooling-to-power ratio. The RTE, exergy efficiency, and *LCOE* of the system were 54.4%, 55.2%, and 170 \$/MWh, respectively.

Besides, Xu et al. [106] proposed a CES-based CCHP system that included a self-evaporating CES subsystem and an ERC, as shown in Fig. 20. This system utilized a flash separator to evaporate CO₂ without requiring an

external heat source. After the flash process, CO₂ was divided into a gas flow and a liquid flow, which were then compressed by the compressor and the pump, respectively. The compression heat was used for heating at temperatures around 180 °C. The ERC utilized waste heat from the expander outlet to generate cooling at 8 °C. Under design conditions, this system could produce 3.9 MW of heating power and 441.4 kW of cooling power, achieving a RTE of 65.0%, an exergy efficiency of 49.3%, and an energy density of 17.5 kWh/m³.

To minimize exergy losses in high-pressure storage, Xu et al. [107] proposed a CES-based CCHP system consisting of an isobaric CES subsystem and a CO₂ heat pump cycle, as illustrated in Fig. 21. In this system, CO₂ was directed through a diverter valve (DV) to both subsystems: the isobaric CES subsystem, which focused on power generation, and the CO₂ heat pump subsystem, which supplied heating via Cooler1 and released cooling (at 6 °C) through Eva2. The RTE of this CES-based CCHP system reached 56.5% under design conditions, and the isobaric supercritical gas storage helped reduce the exergy destruction during CO₂ condensation by 7.7 kJ/kg.

An overview of the performance metrics for CES-based CCHP systems is summarized in Table 4. In addition to the CES-based CCHP systems mentioned earlier, CES systems can also be integrated with carbon capture and power-to-gas technologies to convert CO₂ into valuable products, such as syngas, enabling cross-regional and cross-seasonal energy storage. In these integrated systems, captured CO₂ is typically compressed and stored in high-pressure CO₂ storage tanks, then directed to solid oxide electrolysis cell (SOEC) modules for co-

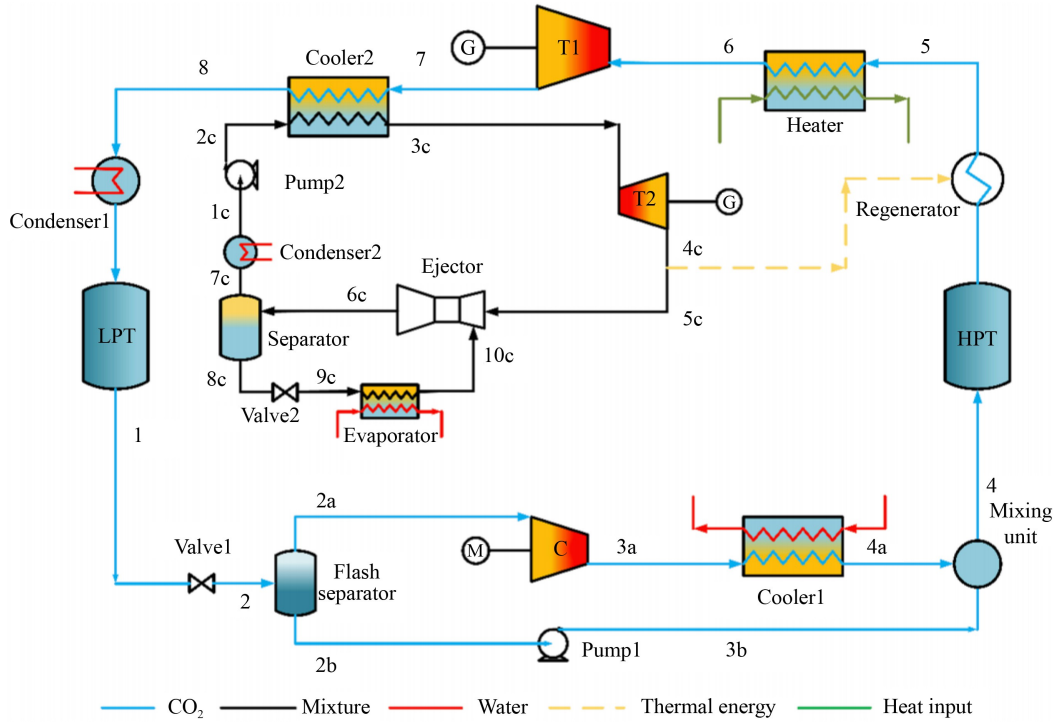


Fig. 20 Schematic diagram of the CES-based CCHP system (HPT: high-pressure tank; LPT: low-pressure tank; C: compressor; T: turbine) (adapted with permission from Xu et al. [106], copyright 2022, Elsevier).

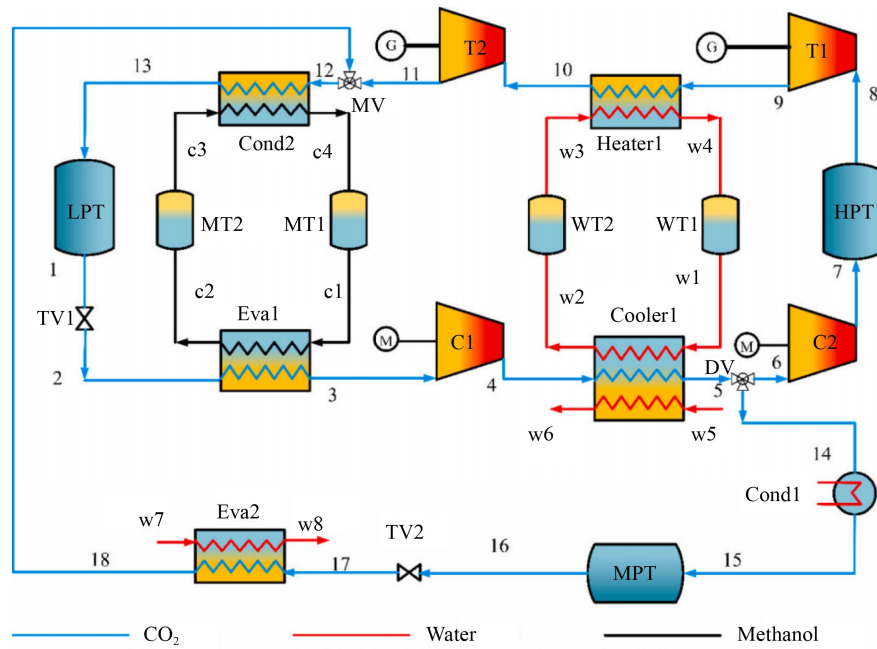


Fig. 21 Schematic diagram of the CES-based CCHP system (DV: diverter valve; Eva: evaporator; HPT: high-pressure tank; LPT: low-pressure tank; HEX: heat exchanger; MT: methanol tank; MPT: moderate-pressure tank; MV: mixing valve; TV: throttle valve; WT: water tank; C: compressor; T: turbine) (adapted with permission from Xu et al. [107], copyright 2024, Elsevier).

electrolysis with high-temperature steam to produce syngas, or to methanation modules for the methanation process using hydrogen from the SOEC modules. Compared to CAES-based CCHP systems, CES-based

CCHP systems are anticipated to function as multi-energy systems, capable of supplying cooling, heating, power, and fuels, providing greater development potential if they are economically viable.

Table 4 Performance metrics of CES-based CCHP systems

Refs.	RET/%	TEE/%	Exergy efficiency/%	Heating temperature/ °C	Cooling temperature/ °C	Economic indicators	Scale
Liu et al. [103]	36	134	–	86 to 244	–24	–	2 MW
Zhang et al. [104]	48	119	–	67	10	–	700 kW
Deng et al. [105]	49	158	51	50	7	<i>LCOE</i> : 100 to 170 \$/MWh	25 MW Charge/discharge period: 6 h
Xu et al. [106]	65	–	49	184	8	<i>LCOE</i> : 68 \$/MWh	10 MW Charge/discharge period: 4 h
Xu et al. [107]	56	–	56	–	6	–	5 MW Charge/discharge period: 6 h

6 Comparative analysis

In this paper, a range of TMES-based CCHP system options were summarized and classified, with a selection of performance indicators defined and to quantify the performance characteristics and relative advantages of various TMES-CCHP systems, an overview of which is shown in Fig. 22. Among the TMES technologies discussed, CAES is currently the most mature and has prompted extensive exploration for CCHP applications, including both basic CAES-based CCHP systems and hybrid CAES-CCHP systems. These systems exhibit RTEs between 23% and 68%, exergy efficiencies between 46% and 66%, and TEEs ranging from 65% to 155%, offering economic advantages over traditional CCHP systems, with approximately 20% lower annual energy supply costs. Furthermore, dynamic operation and control strategies for these systems have shown performance reductions under varying operating conditions. Additionally, given the necessity of including storage volumes for storing high-pressure air, the large-scale implementation of such CAES-based CCHP systems require large air caverns, implying increased storage costs or specific geological conditions.

LAES systems, which typically integrate organic ORC and ARSs technologies to form wider CCHP systems, can achieve RTEs ranging from 40% to 91%, exergy efficiencies between 50% and 61%, and TEEs around 70%. Compared to CAES-based CCHP systems, LAES-based systems store liquid air without the need for caverns, thereby overcoming geographical limitations. However, further research is needed in areas such as dynamic operation, control strategies, and the integration of LAES-based CCHP systems with diverse renewable energy sources and loads.

CCHP systems based on PTES technologies work by direct converting electrical energy into thermal energy for storage, which can then be utilized for heating or cooling. Thermal integration is commonly implemented within ORC-PTES-based CCHP systems to achieve relatively high RTE and TEE (>100%). Furthermore, Joule-Brayton PTES-based CCHP systems feature relatively simple configurations and offer a wide range of heating and cooling capabilities. Cascaded storage allows these systems to supply multi-grade heating and cooling simultaneously,

with RTEs ranging from 58% to 70%, exergy efficiencies between 52% and 85%, and TEEs between 95% and 188%. However, technical challenges remain, such as the development of high-temperature compressors and low-temperature expanders. If these challenges are addressed, Joule-Brayton PTES-based CCHP systems hold the potential to evolve into intelligent energy management systems for urban areas and districts.

CES technology has garnered attention due to the favorable thermodynamic properties of CO₂ and can reduce the requirements for storage. CES-based CCHP systems can achieve RTEs ranging from 36% to 65%, exergy efficiencies around 50%, and TEEs between 119% and 158%. Furthermore, CES systems can also be integrated with carbon capture and power-to-gas technologies, allowing them to produce fuels and evolve into multi-energy management systems capable of supplying cooling, heating, power, and fuels.

Moreover, TMES-based CCHP systems demonstrate significant potential across various applications, including residential and commercial buildings, district heating networks, and industrial processes. Small-scale TMES-based CCHP systems, such as CAES- and LAES-based systems, can be integrated with solar PV or wind energy to meet heating, cooling, and electricity demands in residential and commercial buildings, offering distributed energy solutions such as CAES- and LAES-based CCHP systems. TMES technologies are also well-suited for coupling with district heating networks, where they efficiently store and dispatch thermal energy to complement centralized heating systems. For instance, PTES-based CCHP systems can store surplus thermal energy from power generation and release it during peak heating periods, thereby reducing reliance on fossil fuels. In the industrial sector, LAES-based CCHP systems can provide both cryogenic cooling and electricity, making them ideal for industries such as biopharmaceuticals and data centers, where cooling and power demands are substantial.

7 Summary and outlook

Thermo-mechanical energy storage (TMES) technologies are gaining recognition not only for large-scale and long-term energy storage but also as viable options for

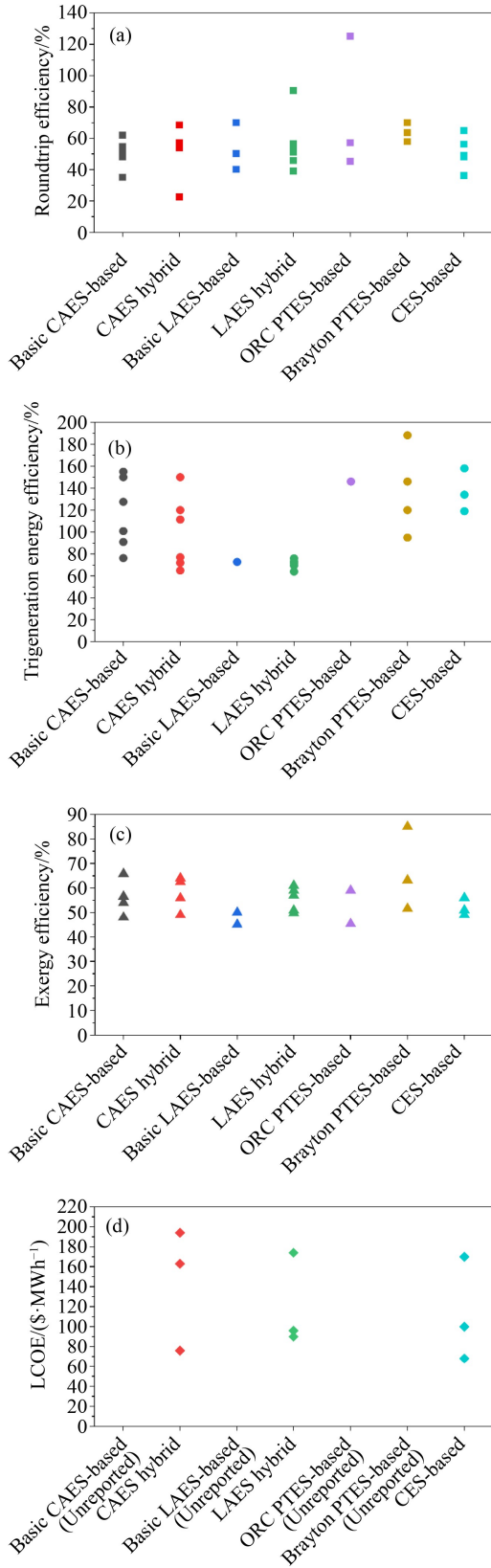


Fig. 22 Evaluation indicators of various TMES-based CCHP systems.

combined cooling, heating, and power provision systems capable of interacting with thermal consumers and/or prosumers. This application is relatively new and topical, with research being more recent and less extensive compared to traditional TMES studies. Analysis and comparison of TMES-based CCHP systems reveal that their RTEs typically range from 40% to 130%, with integration of thermal energy, such as through ORC-PTES-based CCHP systems, leading to significant improvements. The trigeneration energy efficiencies (TEEs) for TMES-based CCHP systems are usually between 70% and 190%, far exceeding the RTE, and further improvements in TEE can be achieved by integrating subsystems such as ORC and ARSs. The LCOE for TMES-based CCHP systems falls between 70 and 200 \$/MWh, although the economic analyses of certain system types, such as PTES-based CCHP systems, remain incomplete.

Among these systems, CAES and LAES technologies, being more mature, are expected to be the first TMES-based CCHP systems to move into demonstration and production phases. PTES-based CCHP systems exhibit the most favorable thermodynamic performance. However, the successful development of high-temperature compressors and low-temperature expanders remains a critical factor that constrains the commercial deployment of these systems, particularly those using the Joule-Brayton cycle type. Additionally, the transcritical CO₂ cycle-based PTES is an important branch of PTES, and its applications in CCHP also require further exploration. Such CO₂-based CCHP systems can be attempted to integrate with carbon capture and power-to-gas technologies to produce fuels, but the thermo-economic feasibility of these systems needs thorough assessment.

Further exploration is necessary to determine optimal TMES-based CCHP system options and configurations for different application scenarios, including the selection and development of key components such as compressors, expanders, and storage units, to facilitate large-scale commercialization. For example, some heat recovery and refrigeration subsystems can be integrated into TMES-based CCHP systems to enhance their thermodynamic performance.

The dynamic nature of CCHP demand throughout the day and year makes the dynamic optimization and control of stored heat and cold essential for effective operation. Advanced control strategies for devices, modules, and systems are essential to ensure reliability in multi-energy supply applications. Moreover, the growing field of “AI for Energy Storage” has gained significant attention. AI-based optimization algorithms and machine learning models can precisely capture the dynamic characteristics of renewable energy and load variations, enabling optimal control of TMES-based CCHP systems and facilitating intelligent management. These AI-driven approaches in energy storage systems can further enhance

efficiency by optimizing charging and discharging cycles, predicting storage demands based on consumption patterns, and extending the lifespan of storage technologies through predictive maintenance.

If these challenges are addressed, these TMES-based CCHP systems hold the potential to evolve into intelligent energy management systems for cities and districts, enabling more sustainable and efficient energy use.

Acknowledgements This work was supported by the National Natural Science Foundation of China (Grant No. 51906150), the Future Foundation of Energy Science (Grant No. WLNYS-2022-010), and the Open Fund Project of State Key Laboratory of Clean Energy Utilization (Grant No. ZJU-CEU2022022), the UK Engineering and Physical Sciences Research Council (EPSRC) (Grant Nos. EP/Y017471/1, and EP/S032622/1). Data supporting this publication can be obtained on request from thameswalker@outlook.com and cep-laboratory@imperial.ac.uk.

Competing Interests The authors declare that they have no competing interest.

References

- Wang Y, Wang R, Tanaka K, et al. Accelerating the energy transition towards photovoltaic and wind in China. *Nature*, 2023, 619(7971): 761–767
- Olabi A G, Onumaegbu C, Wilberforce T, et al. Critical review of energy storage systems. *Energy*, 2021, 214: 118987
- Song H, Liu C, Amani A M, et al. Smart optimization in battery energy storage systems: An overview. *Energy and AI*, 2024: 100378–767
- Mennel J A, Chidambaram D. A review on the development of electrolytes for lithium-based batteries for low temperature applications. *Frontiers in Energy*, 2023, 17(1): 43–71
- Khaljani M, Harrison J, Surplus D, et al. A combined experimental and modelling investigation of an overground compressed-air energy storage system with a reversible liquid-piston gas compressor/expander. *Energy Conversion and Management*, 2021, 245: 114536
- Mersch M, Sapin P, Olympios A V, et al. A unified framework for the thermo-economic optimisation of compressed-air energy storage systems with solid and liquid thermal stores. *Energy Conversion and Management*, 2023, 287: 117061
- Tong Z, Cheng Z, Tong S. A review on the development of compressed air energy storage in China: Technical and economic challenges to commercialization. *Renewable & Sustainable Energy Reviews*, 2021, 135: 110178
- Georgiou S, Shah N, Markides C N. A thermo-economic analysis and comparison of pumped-thermal and liquid-air electricity storage systems. *Applied Energy*, 2018, 226: 1119–1133
- Georgiou S, Aunedi M, Strbac G, et al. On the value of liquid-air and pumped-thermal electricity storage systems in low-carbon electricity systems. *Energy*, 2020, 193: 116680
- White A, Parks G, Markides C N. Thermodynamic analysis of pumped thermal electricity storage. *Applied Thermal Engineering*, 2013, 53(2): 291–298
- Zhao Y, Song J, Liu M, et al. Multi-objective thermo-economic optimisation of Joule-Brayton pumped thermal electricity storage systems: Role of working fluids and sensible heat storage materials. *Applied Thermal Engineering*, 2023, 223: 119972
- Li H, Ding R, Su W, et al. A comprehensive performance comparison between compressed air energy storage and compressed carbon dioxide energy storage. *Energy Conversion and Management*, 2024, 319: 118972
- Qi M, Park J, Landon R S, et al. Continuous and flexible Renewable-Power-to-Methane via liquid CO₂ energy storage: Revisiting the techno-economic potential. *Renewable & Sustainable Energy Reviews*, 2022, 153: 111732
- Li Y, Xu W, Zhang M, et al. Performance analysis of a novel medium temperature compressed air energy storage system based on inverter-driven compressor pressure regulation. *Frontiers in Energy*, 2024, early access
- Cao R, Li W, Ni H, et al. Comprehensive assessment and optimization of a hybrid cogeneration system based on compressed air energy storage with high-temperature thermal energy storage. *Frontiers in Energy*, 2024, early access, doi: 10.1007/s11708-024-0972-2
- Al-Zareer M, Dincer I, Rosen M A. Analysis and assessment of novel liquid air energy storage system with district heating and cooling capabilities. *Energy*, 2017, 141: 792–802
- Esmailion F, Soltani M, Dusseault M B, et al. Performance investigation of a novel polygeneration system based on liquid air energy storage. *Energy Conversion and Management*, 2023, 277: 116615
- Mousavi S B, Ahmadi P, Adib M, et al. Techno-economic assessment of an efficient liquid air energy storage with ejector refrigeration cycle for peak shaving of renewable energies. *Renewable Energy*, 2023, 214: 96–113
- Saher S, Johnston S, Esther-Kelvin R, et al. Trimodal thermal energy storage material for renewable energy applications. *Nature*, 2024(8043): 622–626
- Iqbal Q, Fang S, Xu Z, et al. Techno-economic comparison of high-temperature and sub-ambient temperature pumped-thermal electricity storage systems integrated with external heat sources. *Journal of Energy Storage*, 2024, 89: 111630
- McTigue J D, Farres-Antunez P, J K S, et al. Techno-economic analysis of recuperated Joule-Brayton pumped thermal energy storage. *Energy Conversion and Management*, 2022, 252: 115016
- Iqbal Q, Fang S, Zhao Y, et al. Thermo-economic assessment of sub-ambient temperature pumped-thermal electricity storage integrated with external heat sources. *Energy Conversion and Management*, 2023, 285: 116987
- Qiao H, Yu X, Kong W, et al. Multi-criteria optimization and thermo-economic analysis of a heat pump-organic Rankine cycle Carnot battery system. *Green Energy and Resources*, 2023, 1(4): 100045
- Zhang Y, Liang T, Tian Z, et al. A comprehensive parametric, energy and exergy analysis of a novel physical energy storage system based on carbon dioxide Brayton cycle, low-temperature thermal storage, and cold energy storage. *Energy Conversion*

- and Management, 2020, 226: 113563
25. Steinmann W D. Thermo-mechanical concepts for bulk energy storage. *Renewable & Sustainable Energy Reviews*, 2017, 75: 205–219
 26. Olympios A V, McTigue J D, Farres-Antunez P, et al. Progress and prospects of thermo-mechanical energy storage—A critical review. *Progress in Energy*, 2021, 3(2): 022001
 27. Budt M, Wolf D, Span R, et al. A review on compressed air energy storage: Basic principles, past milestones and recent developments. *Applied Energy*, 2016, 170: 250–268
 28. Venkataramani G, Parankusam P, Ramalingam V, et al. A review on compressed air energy storage—A pathway for smart grid and polygeneration. *Renewable & Sustainable Energy Reviews*, 2016, 62: 895–907
 29. Olabi A G, Wilberforce T, Ramadan M, et al. Compressed air energy storage systems: Components and operating parameters—A review. *Journal of Energy Storage*, 2021, 34: 102000
 30. Bazdar E, Sameti M, Nasiri F, et al. Compressed air energy storage in integrated energy systems: A review. *Renewable & Sustainable Energy Reviews*, 2022, 167: 112701
 31. Borri E, Tafone A, Romagnoli A, et al. A review on liquid air energy storage: History, state of the art and recent developments. *Renewable & Sustainable Energy Reviews*, 2021, 137: 110572
 32. Carraro G, Danieli P, Boatto T, et al. Conceptual review and optimization of liquid air energy storage system configurations for large scale energy storage. *Journal of Energy Storage*, 2023, 72: 108225
 33. Liang T, Zhang T, Lin X, et al. Liquid air energy storage technology: A comprehensive review of research, development and deployment. *Progress in Energy*, 2023, 5(1): 012002
 34. O'Callaghan O, Donnellan P. Liquid air energy storage systems: A review. *Renewable & Sustainable Energy Reviews*, 2021, 146: 111113
 35. She X, Wang H, Zhang T, et al. Liquid air energy storage—A critical review. *Renewable & Sustainable Energy Reviews*, 2025, 208: 114986
 36. Benato A, Stoppato A. Pumped thermal electricity storage: A technology overview. *Thermal Science and Engineering Progress*, 2018, 6: 301–315
 37. Dumont O, Frate G F, Pillai A, et al. Carnot battery technology: A state-of-the-art review. *Journal of Energy Storage*, 2020, 32: 101756
 38. Liang T, Vecchi A, Knobloch K, et al. Key components for Carnot Battery: Technology review, technical barriers and selection criteria. *Renewable & Sustainable Energy Reviews*, 2022, 163: 112478
 39. Vecchi A, Knobloch K, Liang T, et al. Carnot battery development: A review on system performance, applications and commercial state-of-the-art. *Journal of Energy Storage*, 2022, 55: 105782
 40. Cho H, Smith A D, Mago P. Combined cooling, heating and power: A review of performance improvement and optimization. *Applied Energy*, 2014, 136: 168–185
 41. Liu M X, Shi Y, Fang F. Combined cooling, heating and power systems: A survey. *Renewable & Sustainable Energy Reviews*, 2014, 35: 1–22
 42. Zhao Y, Song J, Zhu P, et al. Carnot battery for energy storage: Advancements and challenges. *Green Energy and Resources*, 2023, 1(4): 100048
 43. Lv S, He W, Zhang A F, et al. Modelling and analysis of a novel compressed air energy storage system for trigeneration based on electrical energy peak load shifting. *Energy Conversion and Management*, 2017, 135: 394–401
 44. Tafone A, Borri E, Comodi G, et al. Liquid air energy storage performance enhancement by means of organic Rankine cycle and absorption chiller. *Applied Energy*, 2018, 228: 1810–1821
 45. Li P, Hu Q, Li G, et al. Research on thermo-economic characteristics of a combined cooling, heating and power system based on advanced adiabatic compressed air energy storage. *Journal of Energy Storage*, 2022, 47: 103590
 46. Gao Z, Guo L, Ji W, et al. Thermodynamic and economic analysis of a trigeneration system based on liquid air energy storage under different operating modes. *Energy Conversion and Management*, 2020, 221: 113184
 47. Mignard D. Correlating the chemical engineering plant cost index with macro-economic indicators. *Chemical Engineering Research and Design*, 2014, 92: 285–294
 48. Vieira F S, Balestieri J A P, Matelli J A. Applications of compressed air energy storage in cogeneration systems. *Energy*, 2021, 214: 118904
 49. Liu J L, Wang J H. Thermodynamic analysis of a novel tri-generation system based on compressed air energy storage and pneumatic motor. *Energy*, 2015, 91: 420–429
 50. Arabkoohsar A, Dremark-Larsen M, Lorentzen R, et al. Subcooled compressed air energy storage system for coproduction of heat, cooling and electricity. *Applied Energy*, 2017, 205: 602–614
 51. Kim Y M, Favrat D. Energy and exergy analysis of a micro-compressed air energy storage and air cycle heating and cooling system. *Energy*, 2010, 35(1): 213–220
 52. Facci A L, Sánchez D, Jannelli E, et al. Trigenenerative micro compressed air energy storage: Concept and thermodynamic assessment. *Applied Energy*, 2015, 158: 243–254
 53. Li Y L, Wang X, Li D C, et al. A trigeneration system based on compressed air and thermal energy storage. *Applied Energy*, 2012, 99: 316–323
 54. Cheayb M, Gallego M M, Tazerout M, et al. Modelling and experimental validation of a small-scale trigenenerative compressed air energy storage system. *Applied Energy*, 2019, 239: 1371–1384
 55. Wang M, Bai J, Zhang Z, et al. Assessment of design parameters affecting trigeneration AA-CAES system performance. In: *2020 IEEE 4th Conference on Energy Internet and Energy System Integration*, Wuhan, China, 2020
 56. Alsagri A S, Arabkoohsar A, Rahbari H R, et al. Partial load operation analysis of trigeneration subcooled compressed air energy storage system. *Journal of Cleaner Production*, 2019, 238: 117948
 57. Han Z H, Guo S C. Investigation of operation strategy of combined cooling, heating and power (CCHP) system based on advanced adiabatic compressed air energy storage. *Energy*, 2014, 35: 1–22

- 2018, 160: 290–308
58. Han Z, Sun Y, Li P. Research on energy storage operation modes in a cooling, heating and power system based on advanced adiabatic compressed air energy storage. *Energy Conversion and Management*, 2020, 208: 112573
 59. Han Z H, Guo S C. Investigation of discharge characteristics of a tri-generative system based on advanced adiabatic compressed air energy storage. *Energy Conversion and Management*, 2018, 176: 110–122
 60. Han Z, Sun Y, Li P. Thermo-economic analysis and optimization of a combined cooling, heating and power system based on advanced adiabatic compressed air energy storage. *Energy Conversion and Management*, 2020, 212: 112811
 61. He Y, Zhou S, Xu Y, et al. The influence of charging process on trigenerative performance of compressed air energy storage system. *International Journal of Energy Research*, 2020, 45(12): 17133–17145
 62. Zheng C, Qi X, Yang H, et al. Discharging strategy of adiabatic compressed air energy storage system based on variable load and economic analysis. *Journal of Energy Storage*, 2022, 51: 104403
 63. Arabkoohsar A, Andresen G B. Design and optimization of a novel system for trigeneration. *Energy*, 2019, 168: 247–260
 64. Chen S, Arabkoohsar A, Yang Y, et al. Multi-objective optimization of a combined cooling, heating, and power system with subcooled compressed air energy storage considering off-design characteristics. *Applied Thermal Engineering*, 2021, 187: 116562
 65. Shi K, Asgari A. Energy, exergy, and exergoeconomic analyses and optimization of a novel thermal and compressed air energy storage integrated with a dual-pressure organic Rankine cycle and ejector refrigeration cycle. *Journal of Energy Storage*, 2022, 47: 103610
 66. Liu Z, Liu X, Yang S, et al. Assessment evaluation of a trigeneration system incorporated with an underwater compressed air energy storage. *Applied Energy*, 2021, 303: 117648
 67. Rahbari H R, Arabkoohsar A, Nielsen M P, et al. Quantification of realistic performance expectations from trigeneration CAES-ORC energy storage system in real operating conditions. *Energy Conversion and Management*, 2021, 249: 114828
 68. Liu Z, Yang X, Liu X, et al. Evaluation of a trigeneration system based on adiabatic compressed air energy storage and absorption heat pump: Thermodynamic analysis. *Applied Energy*, 2021, 300: 117356
 69. Ding Y, Olumayegun O, Chai Y, et al. Simulation, energy and exergy analysis of compressed air energy storage integrated with organic Rankine cycle and single effect absorption refrigeration for trigeneration application. *Fuel*, 2022, 317: 123291
 70. Liu Y, Ding Y, Yang M, et al. A trigeneration application based on compressed air energy storage integrated with organic Rankine cycle and absorption refrigeration: Multi-objective optimisation and energy, exergy and economic analysis. *Journal of Energy Storage*, 2022, 55: 105803
 71. Assareh E, Ghafouri A. An innovative compressed air energy storage (CAES) using hydrogen energy integrated with geothermal and solar energy technologies: A comprehensive techno-economic analysis - different climate areas - using artificial intelligent (AI). *International Journal of Hydrogen Energy*, 2023, 48(34): 12600–12621
 72. Assareh E, Keykhal A, Bedakhanian A, et al. Optimizing solar photovoltaic farm-based cogeneration systems with artificial intelligence (AI) and cascade compressed air energy storage for stable power generation and peak shaving: A Japan-focused case study. *Applied Energy*, 2025, 377: 124468
 73. Yun P, Wu H, Alsenani T R, et al. On the utilization of artificial intelligence for studying and multi-objective optimizing a compressed air energy storage integrated energy system. *Journal of Energy Storage*, 2024, 84: 110839
 74. Li P, Hu Q, Han Z, et al. Thermodynamic analysis and multi-objective optimization of a trigenerative system based on compressed air energy storage under different working media and heating storage media. *Energy*, 2022, 239: 122252
 75. Jiang R H, Yin H B, Peng K W, et al. Multi-objective optimization, design and performance analysis of an advanced trigenerative micro compressed air energy storage system. *Energy Conversion and Management*, 2019, 186: 323–333
 76. Li R, Wang H, Zhang H. Dynamic simulation of a cooling, heating and power system based on adiabatic compressed air energy storage. *Renewable Energy*, 2019, 138: 326–339
 77. Sadreddini A, Fani M, Ashjari Aghdam M, et al. Exergy analysis and optimization of a CCHP system composed of compressed air energy storage system and ORC cycle. *Energy Conversion and Management*, 2018, 157: 111–122
 78. Razmi A, Soltani M, Torabi M. Investigation of an efficient and environmentally-friendly CCHP system based on CAES, ORC and compression-absorption refrigeration cycle: Energy and exergy analysis. *Energy Conversion and Management*, 2019, 195: 1199–1211
 79. Razmi A R, Janbaz M. Exergoeconomic assessment with reliability consideration of a green cogeneration system based on compressed air energy storage (CAES). *Energy Conversion and Management*, 2020, 204: 112320
 80. Vecchi A, Li Y, Mancarella P, et al. Multi-energy liquid air energy storage: A novel solution for flexible operation of districts with thermal networks. *Energy Conversion and Management*, 2021, 238: 114161
 81. Peng X D, She X H, Li Y L, et al. Thermodynamic analysis of Liquid Air Energy Storage integrated with a serial system of Organic Rankine and Absorption Refrigeration Cycles driven by compression heat. *Energy Procedia*, 2017, 142: 3440–3446
 82. She X H, Zhang T T, Peng X D, et al. Liquid air energy storage for decentralized micro energy networks with combined cooling, heating, hot water and power supply. *Journal of Thermal Science*, 2021, 30(1): 1–17
 83. Chen X, Chen Y, Fu L, et al. Photovoltaic-driven liquid air energy storage system for combined cooling, heating and power towards zero-energy buildings. *Energy Conversion and Management*, 2024, 300: 117959
 84. Xue X D, Zhang T, Zhang X L, et al. Performance evaluation and exergy analysis of a novel combined cooling, heating and power (CCHP) system based on liquid air energy storage.

- Energy, 2021, 222: 119975
85. Li D, Duan L. Design and analysis of flexible integration of solar aided liquid air energy storage system. *Energy*, 2022, 259: 125004
 86. Ding X, Zhou Y, Zheng N, et al. Energy, exergy, and economic analyses of a novel liquid air energy storage system with cooling, heating, power, hot water, and hydrogen cogeneration. *Energy Conversion and Management*, 2024, 305: 118262
 87. Tafone A, Romagnoli A, Li Y L, et al. Techno-economic analysis of a Liquid Air Energy Storage (LAES) for cooling application in hot climates. *Energy Procedia*, 2017, 105: 4450–4457
 88. Wang C, Akkurt N, Zhang X, et al. Techno-economic analyses of multi-functional liquid air energy storage for power generation, oxygen production and heating. *Applied Energy*, 2020, 275: 115392
 89. Lin X, Sun P, Zhong W, et al. Thermodynamic analysis and operation investigation of a cross-border integrated energy system based on steam Carnot battery. *Applied Thermal Engineering*, 2023, 220: 119804
 90. Poletto C, Dumont O, De Pascale A, et al. Control strategy and performance of a small-size thermally integrated Carnot battery based on a Rankine cycle and combined with district heating. *Energy Conversion and Management*, 2024, 302: 118111
 91. Jockenhöfer H, Steinmann W D, Bauer D. Detailed numerical investigation of a pumped thermal energy storage with low temperature heat integration. *Energy*, 2018, 145: 665–676
 92. Steinmann W D, Bauer D, Jockenhöfer H, et al. Pumped thermal energy storage (PTES) as smart sector-coupling technology for heat and electricity. *Energy*, 2019, 183: 185–190
 93. Lykas P, Bellos E, Korres D N, et al. Energy, exergy, economic, and environmental (4E) analysis of a pumped thermal energy storage system for trigeneration in buildings. *Energy Advances*, 2023, 2(3): 430–440
 94. Chen L, Wang J, Lou J, et al. Thermo-economic analysis of a pumped thermal energy storage combining cooling, heating and power system coupled with photovoltaic thermal collector: Exploration of low-grade thermal energy storage. *Journal of Energy Storage*, 2024, 96: 112718
 95. Zhang H, Wang L, Lin X, et al. Combined cooling, heating, and power generation performance of pumped thermal electricity storage system based on Brayton cycle. *Applied Energy*, 2020, 278: 115607
 96. Zhao Y, Song J, Zhao C, et al. Thermodynamic investigation of latent-heat stores for pumped-thermal energy storage. *Journal of Energy Storage*, 2022, 55: 105802
 97. Zhao Y, Xie Y, Song J, et al. Second-law thermodynamic assessment of cascaded latent-heat stores for pumped-thermal electricity storage. *Applied Thermal Engineering*, 2025, 262: 125290
 98. Zhao Y, Huang J, Song J, et al. Thermodynamic investigation of a Carnot battery based multi-energy system with cascaded latent thermal (heat and cold) energy stores. *Energy*, 2024, 296: 131148
 99. Huang J, Zhao Y, Song J, et al. Thermodynamic investigation of a Joule-Brayton cycle Carnot battery multi-energy system integrated with external thermal (heat and cold) sources. *Applied Energy*, 2025, 377: 124652
 100. Alsagri A S. An innovative design of solar-assisted Carnot battery for multigeneration of power, cooling, and process heating: Techno-economic analysis and optimization. *Renewable Energy*, 2023, 210: 375–385
 101. Wang H N, Xue X J, Zhao C Y. Performance analysis on combined energy supply system based on Carnot battery with packed-bed thermal energy storage. *Renewable Energy*, 2024, 228: 120702
 102. Zheng P, Hao J, Zhang Z, et al. Analysis of heat transfer characteristics of a novel liquid CO₂ energy storage system based on two-stage cold and heat storage. *Frontiers in Energy*, 2024, early access
 103. Liu Z, Cao F, Guo J, et al. Performance analysis of a novel combined cooling, heating and power system based on carbon dioxide energy storage. *Energy Conversion and Management*, 2019, 188: 151–161
 104. Zhang Y, Lin Y, Lin F, et al. Thermodynamic analysis of a novel combined cooling, heating, and power system consisting of wind energy and transcritical compressed CO₂ energy storage. *Energy Conversion and Management*, 2022, 260: 115609
 105. Deng Y, Wang J, Cao Y, et al. Technical and economic evaluation of a novel liquid CO₂ energy storage-based combined cooling, heating, and power system characterized by direct refrigeration with phase change. *Applied Thermal Engineering*, 2023, 230: 120833
 106. Xu W, Zhao P, Gou F, et al. Thermo-economic analysis of a combined cooling, heating and power system based on self-evaporating liquid carbon dioxide energy storage. *Applied Energy*, 2022, 326: 120032
 107. Xu W, Zhao P, Ma N, et al. Design and performance analysis of a combined cooling, heating and power system: Integration of an isobaric compressed CO₂ energy storage and heat pump cycle. *Journal of Energy Storage*, 2024, 91: 112146